CrystEngComm

HIGHLIGHT

View Article Online
View Journal | View Issue

Cite this: *CrystEngComm*, 2025, **27**, 7460

Received 30th July 2025,
Accepted 13th October 2025

DOI: 10.1039/d5ce00761e

rsc.li/crystengcomm

Recent advances in five-coordinate Co(II) single-ion magnets

Atanu Dey, *[a] Soumalya Roy[b] and Sourav Das *[c]

This review summarizes recent advances in five-coordinate Co(II) single-ion magnets (SIMs) with trigonal bipyramidal and square pyramidal geometries, highlighting the influence of these geometries on magnetic anisotropy and magnetization dynamics. The insights presented in this review provide a strong foundation for the strategic design of ligand environments surrounding the Co(II) center. By understanding the interplay between geometries and electronic structures, researchers can strategically tune the ligand field strength to modulate magnetic anisotropy and exert precise control over the overall magnetic behavior.

Introduction

Single-molecule magnets (SMMs) have been the focus of research for close to three decades because of their potential technological applications in areas such as high-density data storage, (nano)spintronics, and quantum computing.[1–6] One of the salient features of these molecular architectures is slow magnetization relaxation, leading to magnetic hysteresis below a blocking temperature, typically in the temperature range of liquid helium.[7] This behavior is notably observed even in the absence of an external magnetic field, a phenomenon linked to zero-field splitting (ZFS).[8] The origin of ZFS lies in spin–orbit coupling, which removes the degeneracy of the magnetic sublevels ($\pm M_S$) of the ground spin state (S), forming an energy barrier that hinders spin reversal.

The height of this barrier and the dynamics of spin relaxation are primarily determined by the magnitude and nature of magnetic anisotropy, whether axial, rhombic, Ising-type, or planar. When the axial zero-field splitting parameter D is negative, the system has easy-axis anisotropy such that the highest M_S components occupy the lowest in energy. However, for easy-plane anisotropy, a positive D value defines an easy-plane such that the lowest M_S values describe the ground state. The effective energy barrier against magnetization reversal (U_{eff}) in the case of easy-axis systems scales approximately with $|D|$, whereas the tunneling probability among M_S levels depends on the rhombic anisotropy parameter E.[9,10]

The initial report of the SMM prototype, $[Mn^{III}{}_8Mn^{IV}{}_4O_{12}(O_2CCH_3)_{16}(H_2O)_4]$ (Mn_{12}–Ac), commonly known as Mn_{12}–acetate, was originally reported by Prof. Lis in 1980.[11] Its substantial spin ground state (S = 10), which is stabilized by the axial distortion of Mn^{III} ions, established the foundation for the field.[12,13] However, attempts to further improve the total spin of these systems tended to result in lower overall anisotropy owing to the stronger magnetic interactions between the metal centers. An example of a complex $[Mn^{III}{}_6O_2(sao)_6(O_2CPh)_2(EtOH)_4]$ (Mn_6; S = 4) was provided by Brechin, Christou, and co-workers, which showed a transition metal cluster with an 86 K record energy barrier but with a relatively low axial anisotropy parameter ($|D|$ = 0.62 K), reflecting the difficulty of simultaneous optimization of both spin and anisotropy.[14–16] This complexity has resulted in a strategic emphasis on mononuclear systems, where magneto-structural correlations can be more precisely tuned using rational ligand design and electronic structure considerations.[17–20] These systems provide more predictable structure–property relationships,[21] making them easier to manipulate in solution and on the surface.[22,23] While lanthanide-based SIMs leverage strong spin–orbit coupling and large magnetic moments, transition metal SIMs rely more on subtle electronic properties. The magnetic anisotropy in these systems originates from the zero-field splitting (ZFS) of spin sub-levels in the ground state, which is often controlled by spin–orbit coupling and the effect of the surrounding ligand field.[24–26] For any given metal ion, the presence of unquenched orbital angular momentum or the second-order mixing of excited states into the ground state through geometry-dependent spin–orbit coupling influences the magnitude and direction of magnetic anisotropy.[27] When these effects combine with a high-spin ground state ($S > 1/2$), a spin-reversal barrier can arise, enabling slow magnetization

[a] *Industrial Chemical Product Development and Analysis Centre, Department of Chemistry, Gandhi Institute of Technology and Management (GITAM), NH 207, Nagadenehalli, Doddaballapur Taluk, Bengaluru, 561203 Karnataka, India. E-mail: adey2@gitam.edu, atanu130@gmail.com*
[b] *Department of Chemistry, Chonnam National University, 77 Yongbong-ro, Buk-gu, Gwangju 61186, Republic of Korea*
[c] *Department of Basic Sciences, Chemistry Discipline, Institute of Infrastructure, Technology, Research And Management (IITRAM), Near Khokhra Circle, Maninagar East, Ahmedabad-380026, Gujarat, India. E-mail: souravdas@iitram.ac.in*

relaxation. Consequently, the design of transition-metal SIMs involves a subtle trade-off between the electronic structure, coordination geometry, and ligand field effects.[28–30] Therefore, the study focused on modifying the D values associated with mononuclear metal complexes. In this area of interest, Long and coworkers were the first to introduce a transition metal-based single-ion magnet (SIM) in 2010. This SIM is defined by the molecular formula of K[Fe(^{tpa}Mes)] (^{tpa}Mes = mesityltripyroleamine) and features a trigonal pyramidal geometry around Fe(II) with a D value of −39.6 cm^{-1}.[31] This discovery paved the way for exploring the magnetic anisotropy of other transition metal complexes, particularly those involving the Co(II) ion, which can demonstrate both substantial negative (easy-axis) and large positive (easy-plane) magnetic anisotropy (D), depending upon its coordination environment.[32–34] This phenomenon has been observed across a spectrum of coordination numbers ranging from two to eight, encompassing tetrahedral, octahedral, and notably penta-coordinate structures, as well as rare geometries such as trigonal prismatic, trigonal planar (CN = 3), linear (CN = 2), and higher-coordinate environments, including seven- or eight-coordinate complexes.[24] Among these diverse structures, penta-coordinate Co(II) complexes are particularly noteworthy, since they can adopt geometries ranging from trigonal bipyramidal to square pyramidal forms, each influencing the zero-field splitting (ZFS) parameters and thereof magnetic relaxation dynamics.[35] The Co(II) system with a trigonal bipyramidal (TBP) geometry generally tends to favor a positive D value. Conversely, square pyramidal (SPY) configurations often stabilize large negative D values, which leads to preference for SIM behavior in the absence of a magnetic field. To close the gap between geometric configuration and magnetic characteristics, researchers have developed a parameter to describe the geometry of pentacoordinate complexes. This parameter, known as the Addison τ parameter, quantifies the geometric structure, where $\tau \approx 1$ corresponds to TBP and $\tau \approx 0$ indicates SPY-like structures.[36] It is intriguing that Co(II) complexes with geometries that lie between the two extremes have not been extensively explored, even though they display unique magnetic characteristics due to subtle distortions and ligand field influences. These distortions impact the axial (D) and rhombic (E) anisotropy components, thereby influencing the spin relaxation barrier.[8] The application of theoretical models to these systems can provide a more comprehensive understanding of their electronic structures.[37–39] By delving deeper into the electronic properties of these systems, theoretical frameworks like the spin-Hamiltonian (SH) formalism for orbitally nondegenerate ground states and the Griffith–Figgis (GF) approach for orbitally degenerate states provide insights into the electronic structures that cause anisotropy. For instance, SH parameters such as D and E characterize ZFS in compressed octahedral and ideal TBP geometries, whereas GF parameters such as the spin–orbit coupling constant (ξ) and orbital reduction factor (κ) are required for systems with degenerate ground terms.[40,41]

Given the unique ability of five-coordinated Co(II) complexes to reveal tunable magnetic anisotropy through subtle geometric and electronic alterations, they represent an ideal platform for advancing the understanding and design of high-performance single-ion magnets (SIMs). The recent literature has shown promising relationships between the coordination geometry, especially between the trigonal bipyramidal and square pyramidal, and the magnetism observed. This review is an attempt to bring together some of the most recent advances in this newly developing field, concentrating on the structural, spectroscopic, and theoretical means of approaching the design of five-coordinated Co(II)-based SIMs. Through the critical examination of some keystone papers, we aim to shed light on current trends, open challenges, and potential areas of research in the rational design of transition metal-based molecular magnets.

Magnetic anisotropy in Co^{II}-complexes

In a paramagnetic transition metal complex, the energy levels of the spin states are governed by four factors: i) electron–electron repulsions, ii) the ligand field strength around the metal center, iii) spin–orbit coupling, and iv) spin–spin interactions. For a free ion with a d^n electron configuration, the associated spectroscopic term symbols are expressed as ^{2S+1}L, where L is the total orbital angular momentum quantum number and S is the total spin quantum number.[8,25,30,42]

A relativistic effect associated with magnetic anisotropy—namely, zero-field splitting (ZFS)—lifts the degeneracy of the ground-state M_S components even in the absence of an external magnetic field ($H = 0$). This splitting occurs without the application of any magnetic field; therefore, it is referred to as zero-field splitting. ZFS represents the removal of spin degeneracy in microstates for systems with total spin $S > 1/2$ at zero magnetic field. It is a key contributor to magnetic anisotropy in 3d transition metal complexes. This phenomenon is typically described using the following spin Hamiltonian: $H = D[S_z^2 - S(S+1)] + E(S_x^2 - S_y^2)$, where D and E are the axial and rhombic zero-field splitting parameters, respectively, and S_x, S_y, and S_z are the spin operators along the respective axes.[8] In an odd-electron system, the axial zero-field splitting parameter (D) lifts the degeneracy of the spin microstates, leading to the formation of Kramers doublets. The rhombic parameter (E) further splits these doublets, thereby introducing transverse anisotropy. The primary origin of zero-field splitting (ZFS) is the spin–orbit coupling (SOC), which arises from the interaction between the electron's spin and its orbital angular momentum. The spin–orbit coupling (SOC) is primarily influenced by the coupling between the ground electronic state and nearby excited states. Nevertheless, the electronic configuration and energy gaps between these states play critical roles in determining the magnitude of D. A larger D value generally corresponds to a smaller energy separation between the

ground and excited states. Among these, the strongest contribution to D typically arises from the spin–orbit coupling with the first excited state, as its proximity allows for a more effective interaction with the ground state. Additionally, spin–spin or spin–dipolar interactions also contribute to ZFS, but their magnitude is typically negligible and they mainly induce rhombic anisotropy (E).[26]

Spin–orbit coupling (SOC) contributes to zero-field splitting (ZFS) through two primary mechanisms: in-state (first-order) SOC and out-of-state (second-order) SOC. In-state SOC arises when the ground electronic state retains substantial orbital angular momentum, enabling direct spin–orbit interactions that lead to significant ZFS. In contrast, out-of-state SOC becomes relevant when the ground state is orbitally nondegenerate (*i.e.*, lacks orbital angular momentum), but can couple—through SOC—with nearby excited states that do possess orbital angular momentum. This second-order interaction also induces ZFS, though its magnitude is generally smaller compared to the first-order contribution.[30,33]

A classic example of first-order spin–orbit coupling (SOC) is found in Co(II), a d^7 ion with the ^4F Russell–Saunders ground electronic state. In a weak octahedral crystal field, this term splits into the $^4T_{1g}$ ground state, followed by the $^4T_{2g}$ and $^4A_{2g}$ first and second excited states, respectively. In octahedral symmetry, the ground term is $^4T_{1g}$, which possesses an in-state orbital contribution and leads to strong first-order SOC. In an octahedral ligand field, the ground term $^4T_{1g}$ possesses an inherent orbital angular momentum, resulting in significant first-order spin–orbit coupling (SOC) that splits the $^4T_{1g}$ state into three spin–orbit-coupled levels (J = 5/2, J = 3/2, and J = 1/2). However, achieving strict octahedral symmetry is rare in real systems. The most commonly observed geometry for Co(II) is an axially distorted octahedron (D_{4h}). This distortion lifts the degeneracy of the $^4T_{1g}$ ground term, splitting it into $^4A_{2g}$ and ^4E_g states. Subsequent SOC interactions further divide these into six Kramers doublets corresponding to J = 1/2 (M_J = ±1/2), J = 3/2 (M_J = ±1/2, ±3/2), and J = 5/2 (M_J = ±1/2, ±3/2, ±5/2), yielding a system with potentially strong magnetic anisotropy (Fig. 1).[33]

The magnetic quantum numbers (m_l) for the five d-orbitals are assigned as follows: m_l = 0 for d_{z^2}, m_l = ±1 for d_{xz} and d_{yz}, and m_l = ±2 for d_{xy} and $d_{z^2-y^2}$. In metal complexes, the sign of D is determined by the magnetic quantum number (m_l) of the orbitals involved in the spin transition, while the magnitude of D is governed by the energy gap between these orbitals. Transitions between orbitals having the same m_l values (spin-allowed transitions) typically result in a negative D value, whereas transitions between orbitals with different m_l values generally produce a positive D value.[26]

Five-coordinate transition metal complexes typically adopt either a trigonal bipyramidal (TBP) or square pyramidal geometry. Although the ideal TBP geometry with D_{3h} symmetry is scarce, distorted TBP with C_{3v} symmetry is the most commonly observed. In the distorted TBP geometry, a high-spin Co(II) (d^7 configuration) ion exhibits an electronic configuration where four electrons occupy the lower-energy d_{yz} and d_{xz} orbitals, with one electron in each of the remaining three d orbitals. Consequently, the first excited quartet state arises from the promotion of an electron from d_{yz}/d_{xz} to the d_{xy} orbital. Since this involves a change in the magnetic quantum number (m_l), this leads to a positive D value. In contrast, for square pyramidal geometries (with C_{4v} symmetry), the sign of the D parameter depends on the ligand field strength of the coordinating atoms/ligands. When the ligands are strong π-donors, they stabilize Co(II) in the *xy* plane, favoring orbital interactions that contribute to a positive D value. In contrast, strong σ-donor ligands tend to pull Co(II) out of the *xy*-plane, which typically results in a negative D value owing to different orbital overlaps (Fig. 2). Nonetheless, the actual magnitude of D is determined by all contributions influencing the effective energy diagram of the d orbitals, which in turn depends on both structural and chemical factors.[26,43]

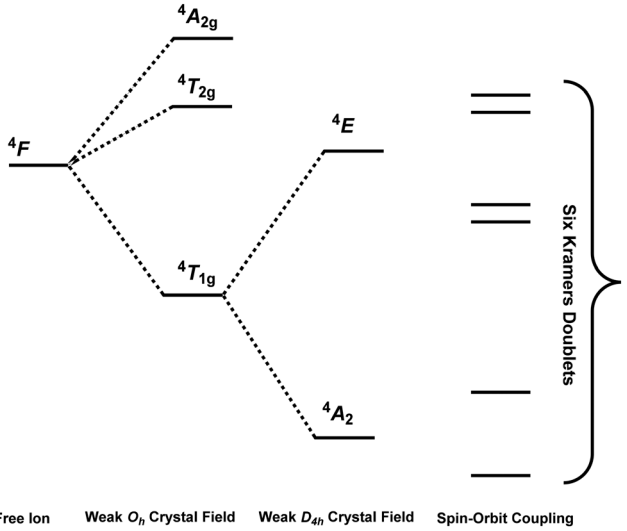

Fig. 1 Schematic energy level diagram illustrating the splitting of the ^4F term under an octahedral ligand field, followed by the in-state spin–orbit coupling-mediated splitting of the resulting triplet term, adapted/reproduced from ref. 33 with permission from The Royal Society of Chemistry,[33] copyright 2016.

Magnetic anisotropy parameters can be determined using various methods, with the most common being the fitting of magnetic measurements—such as direct current (dc) susceptibility and variable-field magnetization at low temperatures.[44,45] However, these techniques may not always yield accurate values, as the experimental data can be insensitive to the sign and, at times, even the magnitude of the axial zero-field splitting (D) parameter. For more reliable determination of ZFS parameters, advanced characterization techniques such as high-field/high-frequency electron paramagnetic resonance (EPR), nuclear magnetic resonance (NMR) paramagnetic shift analysis, variable-field terahertz (THz) spectroscopy, inelastic neutron scattering (INS), far-infrared spectroscopy, and torque magnetometry can be

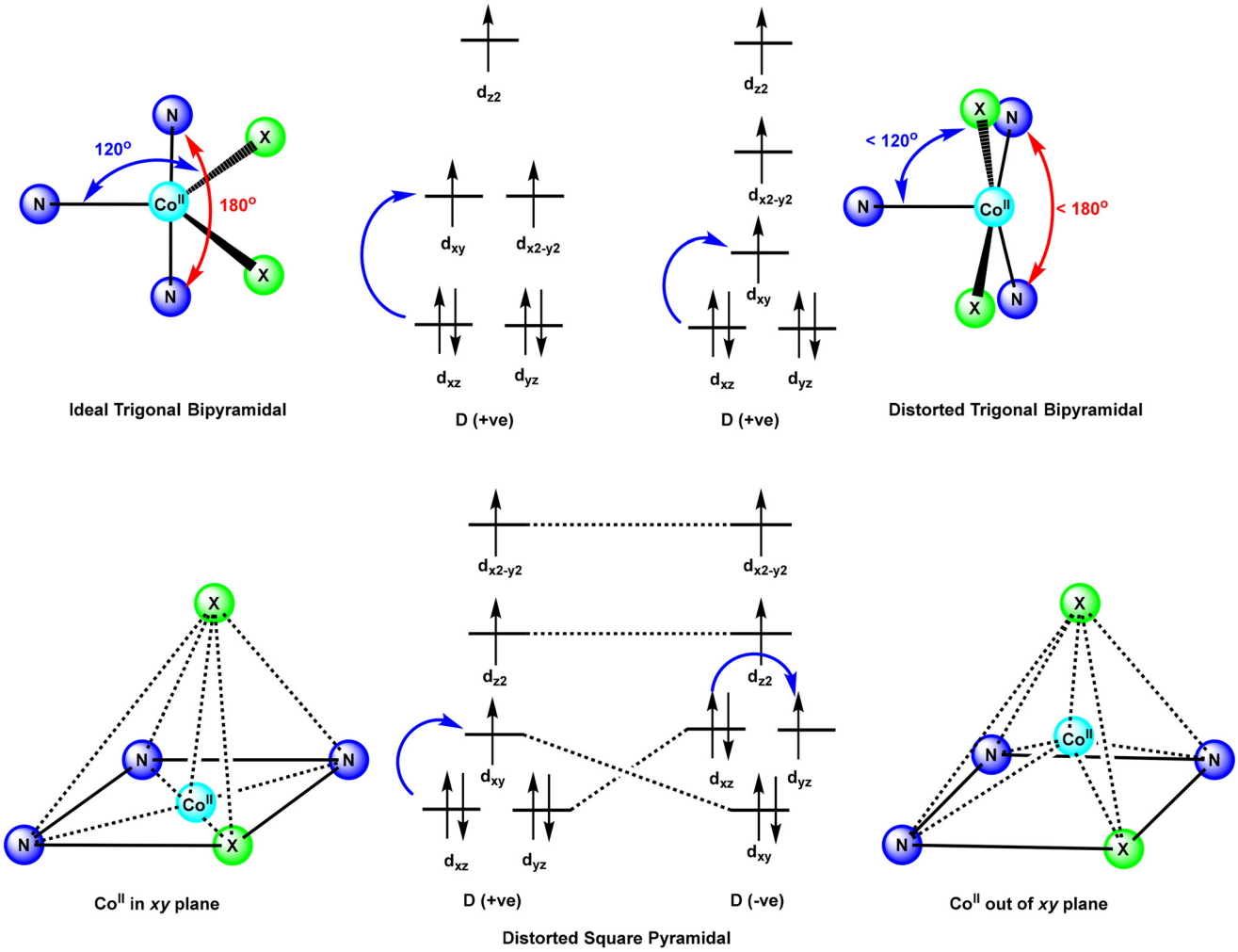

Fig. 2 Qualitative d-orbital splitting diagrams for TBP (top) and square pyramidal (bottom) geometries, adapted/reproduced from ref. 46 with permission from Wiley,[46] copyright 2020 and modified.

employed. In addition, theoretical methods based on wavefunction-based techniques, including SA-CASSCF, CASSCF/NEVPT2, CASPT2, *etc.* offer valuable and often reliable estimates of these parameters.[46–49] CASSCF/NEVPT2 computation methods stand out as the most effective for capturing spin–orbit coupling and identifying anisotropy axes. Yet, with all their benefits, the CASSCF/NEVPT2 method falls short as the trustability of outcomes depends on practices such as the chosen active space, basis set, and dynamic correlation approach. The same is valid for other methods of analysis. While AILFT offers insightful orbital interpretations by recourse to *ab initio* ligand field theory, it depends on the projection scheme used on the multireference wavefunction. Spin Hamiltonian methods of retrieving magnetic parameters are simple and easy to use but may not capture the complexity of anisotropic interactions, especially in the presence of significant transverse anisotropy. It is thus essential to consider the impacts of the employed methods in the evaluation of the results and to complement the analyses from computations with the analyses from experiments.[50–52] By explicitly noting these considerations, a more balanced and reproducible framework can be established for connecting theory with experiment in Co(II)-based SIMs.

Quantum tunneling of magnetization (QTM) remains a major barrier to advancing the field of SMMs, as it facilitates rapid loss of magnetization and limits their effectiveness for applications. To improve the performance of SMMs, it is essential to suppress relaxation processes, especially QTM. Some of the well-known are: (a) tuning the ligand field to boost Ising type anisotropy and/or preserving higher molecular symmetry to avoid wave function mixing and encourage relaxation through higher excited states, (b) applying a direct current (dc) magnetic field to lift the degeneracy of the $\pm M_J/\pm M_S$ ground states, (c) employing magnetic dilution to reduce dipolar interactions among paramagnetic centers and hyperfine coupling with nuclear spins, (d) choosing an appropriate Kramers ion, *etc.* Since QTM results from transverse anisotropy that facilitates tunneling between superposed doublets, reducing this transverse component further helps in suppressing QTM.[53–56] Among the wide range of single-ion magnets (SIMs) based on

3d transition metal ions, Co(II)-based complexes have garnered significant attention due to several compelling reasons: (i) their ability to adopt a variety of stable coordination geometries, typically from four to eight, (ii) the frequent occurrence of high-spin configurations in their native state (commonly $S = 3/2$), and (iii) being a Kramers ion ($S = 3/2$), Co(II) possesses degenerate spin ground states in the absence of an external magnetic field, providing an inherent advantage in minimizing quantum tunneling of magnetization (QTM).[35,57] Additionally, in a complex exhibiting Ising-type anisotropy with a half-integer spin (Kramers ion), the reversal of magnetization primarily occurs through thermally activated over-barrier relaxation mechanisms, as quantum tunneling processes are suppressed due to the spin parity effect enforced by Kramers degeneracy at zero magnetic field.[58,59] This is because quantum tunneling of magnetization (QTM) is strongly suppressed at zero external magnetic field, a consequence of spin parity effects and Kramers degeneracy which prevent direct tunneling between the ground doublet states in the absence of a field. These attributes make Co(II) a particularly attractive candidate for designing 3d-based SIMs. Accordingly, this review focuses on the influence of various ligand field strength in modulating the zero-field splitting (ZFS), and consequently, the sign and magnitude of magnetic anisotropy in penta-coordinated Co(II) complexes.

Mechanism of slow magnetization relaxation

Magnetic relaxation is the process where a magnetic moment, or spin, changes its direction to align with an applied magnetic field. When the spin is not aligned with the field, it is in an excited state, and the lowest energy state is when the spin is aligned with the field. Essentially, magnetic relaxation is the spin moving from a higher energy orientation to a more stable, lower energy alignment with the magnetic field. In principle, if the magnetization relaxation could only occur by overcoming the full energy barrier through all excited states, any magnetic material is expected to have an U_{eff} ~298 K (~207 cm^{-1}) at room temperature.[60] However, due to the quantum nature of these materials, relaxation mechanisms are complex and influenced by temperature, magnetic field, hyperfine interactions (between electronic and nuclear spins), and intermolecular forces. The major relaxation pathways in SMMs include spin-phonon (lattice) coupling processes that consist of Orbach, Raman, and direct mechanisms and quantum mechanisms such as QTM and thermally assisted QTM (TA-QTM) (eqn (1)).[55,60,61] The Orbach and Raman processes involve two phonons, while the direct process involves a single phonon. These diverse mechanisms contribute to the complexity and sensitivity of relaxation dynamics in SMMs. Spin-lattice relaxation is the process where a spin returns to alignment with the applied magnetic field by exchanging energy with its surroundings, known as the lattice. Specifically, it describes how a spin relaxes from a higher energy spin-up state (less stable) to the lower energy spin-down state (more stable), reaching equilibrium with the environment. Unlike the Orbach and Raman processes that involve two phonons interacting simultaneously, the direct relaxation process is assisted by just a single phonon facilitating the transition.[62]

The Orbach process involves exciting the spin from its initial state ($M_s = \pm S$) to a higher energy spin state ($M_s = 0$) using energy from a phonon [$(h/2\pi) \times \omega_1$]. This excited spin state acts as an effective transition state. The relaxation then happens as the spin moves from this higher energy state back to a lower energy orientation by releasing energy to the lattice [$(h/2\pi) \times \omega_2$], also in the form of a new phonon. This process can include multiple steps, where the spin is excited through several higher energy states before relaxing by phonon emission. For the process to occur, phonons with the right energy must be available to excite the spin to these transition states. The energy difference between the phonon absorbed and the phonon emitted corresponds to the energy gap between the $\pm M_S$ sublevels in the ground state. Typically, Orbach relaxation does not proceed through the highest excited state, but rather through the intermediate excited states.

In the direct process, the spin transitions straight from the initial to the final orientation because the energy difference between the two spin levels matches the energy of a lattice phonon. This means the process bypasses any intermediate transition states entirely. The Raman relaxation process occurs through a virtual excited state through inelastic dispersion of phonons, where a spin system simultaneously absorbs $(h/2\pi) \times \omega_3$ and emits phonons $(h/2\pi) \times \omega_4$ with different energies (Fig. 3). This is fundamentally different from the direct process, which involves the emission of only one phonon, and from the Orbach process, which involves sequential absorption followed by emission of phonons. In addition to energy exchange with phonons from the environment, QTM allows the spin to relax by tunneling directly through the energy barrier instead of going over it. This quantum process bypasses thermal activation, enabling magnetization relaxation without phonon involvement. This quantum mechanical effect enables magnetization relaxation without needing thermal activation or phonon interaction. QTM-based processes are of two types. The first, called "ground-state" QTM, occurs directly between the initial and final spin orientations without requiring any input energy. This happens when a magnetic interaction between the wavefunctions of these spin states creates a tunnel-splitting energy gap, Δ_T in the barrier. The second process, thermally assisted QTM, needs energy exchange with the lattice. It starts with a phonon promoting the spin to a higher-energy M_S level below the highest excited state for systems with $S > 1/2$. From this excited state, the spin tunnels through the barrier to another M_S level before finally relaxing to its ground orientation. In general, several relaxation processes can coexist within a system, with each one dominating in a specific temperature range. Processes such as QTM and

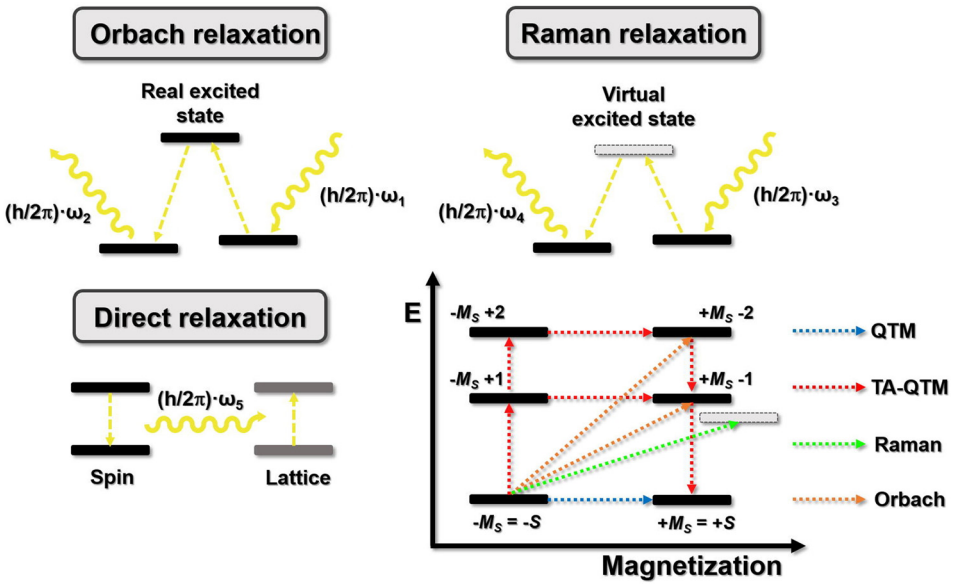

Fig. 3 A schematic illustrating the three main magnetization relaxation mechanisms: Orbach (top left), Raman (top right), and direct (bottom left). Additionally, a combination of various relaxation pathways, including QTM and thermally assisted QTM (TA-QTM) is depicted (bottom right),[60] adapted/reproduced from ref. 60 with permission from Elsevier,[60] copyright 2021.

direct relaxation typically dominate at low temperatures, while the Orbach mechanism operates at higher temperatures and TA-QTM at intermediate ranges. In contrast, the Raman process can contribute across the entire temperature spectrum. Among these mechanisms, QTM and TA-QTM are regarded as "through-barrier shortcuts", since relaxation occurs without surmounting the barrier. As a result, the apparent barrier height U is reduced, leading to an effective energy barrier U_{eff}. This reduction directly impacts both the blocking temperature and the relaxation time. AC magnetic susceptibility measurements are a key technique for probing slow magnetization relaxation, enabling the determination of τ at various temperatures. By fitting the temperature dependence of τ [$\ln(\tau)$ *vs.* T^{-1}] with the appropriate equation, one can extract parameters associated with the different relaxation mechanisms, including U_{eff}.[55]

$$\tau(T, H)^{-1} = \tau_{\text{Orbach}}(T)^{-1} + \tau_{\text{Raman}}(T)^{-1} + \tau_{\text{direct}}(T, H)^{-1} + \tau_{\text{QTM}}(H)^{-1} \quad (1)$$

It is important to mention from eqn (1) that the relaxations are field dependent and applying an external magnetic field can suppress QTM by decreasing the overlap of quasi-degenerate states, while simultaneously favoring the direct relaxation process. Nevertheless, the relaxation process is governed by multiple factors, including the strength and symmetry of the ligand field, spin state, isotopic composition, hyperfine and intermolecular interactions, presence of nearby magnetic species, temperature, and applied magnetic field.[53] Gaining a deep understanding of the underlying relaxation mechanisms is essential for optimizing the performance of SMMs.

Synthetic strategies for five-coordinate Co(II) SIMs

Recent work has demonstrated that five-coordinate Co(II) environments can be systematically tuned through diverse synthetic approaches. Tripodal phenolate/amine scaffolds give rise to the distorted trigonal-bipyramidal or square pyramidal sites where the zero-field splitting and the field-induced slow relaxation are functions of subtle geometric changes as corroborated by theoretical calculations.[34,35,57] Substitution of halides in square pyramidal complexes (Cl, Br, and I) gives rise to large and tunable easy-axis D values, demonstrating the control of axiality and relaxation pathways by anionic co-ligands.[63] The aza-macrocyclic ligands impose penta-coordination, producing mononuclear Co(II) complexes with field-induced slow relaxation and demonstrating the macrocycle design as a tool to control the geometry and the dynamics.[64] Controlled crystallization also makes it possible to access axial and equatorial isomers of borohydride complexes, where isomerism leads to different g-values and relaxation mechanisms with Raman *versus* QTM contributions.[65] All these approaches demonstrate that tuning the shape of Co(II) single-ion magnets goes beyond mere ligand field engineering. It also involves the strategic selection of halides, alteration of the ligand field strength, and modifications at the framework level offering multiple avenues to control magnetic anisotropy and relaxation dynamics.

Five coordinated Co(II) complexes

Although six-coordinated geometries are generally preferred by 3d transition metal ions due to their tendency toward

coordination saturation, stable five-coordinate metal complexes are also frequently encountered.[66] These penta-coordinated species typically adopt distorted trigonal bipyramidal (C_{3v} symmetry) or distorted square pyramidal geometries (C_{4v} symmetry). This section highlights various examples of Co(II)-based single-ion magnets (SIMs) featuring different coordination environments and symmetries. For clarity, we have divided the discussion into two parts. The first part focuses on Co(II) complexes with an $NNNX_2$ ('NNN' denotes the donor atoms from the ligand backbone, whereas 'X' represents halide or pseudohalide anions coordinated to the metal center) coordination environment, while the second part covers five-coordinate Co(II) complexes exhibiting alternative coordination geometries other than $NNNX_2$. The extent of distortion from the ideal geometry, including the displacement of the Co(II) ion from the basal plane (δ) and the anisotropy parameters (D), is shown in the respective figures. A more detailed summary of the geometrical features and magnetic properties is provided in the corresponding tables.

Complexes with a formula of Co(II)(NNN)X_2

The first single ion magnet based on the Co(II) ion was reported by Richeson and coworkers using bis(imino)pyridine NNN-pincer ligands (L^1); $[Co^{II}(L^{1a/1b})(SCN)_2]$ complexes, R = Me (**1a**) or Ph (**1b**) (Fig. 4). In both complexes, the Co(II) center exhibits a distorted square pyramidal geometry, coordinated by three nitrogen donors from the NNN-ip ligand and one monodentate SCN ligand in the basal plane, with the second SCN ligand occupying the axial position. The Co(II) ion in complex **1a** is displaced by 0.39 Å above the basal plane, whereas in **1b**, the displacement increases to 0.52 Å. This out-of-plane shift is proposed to enhance spin–orbit coupling, which can be strategically utilized to modulate magnetic anisotropy. The resulting electronic structure of these complexes is influenced by this displacement. Notably, both complexes exhibit easy-axis magnetic anisotropy with $D \sim -28.2$ cm^{-1}. Both the complexes exhibited field induced SIM behavior (under an applied field of 2000 Oe) with the following characteristics:

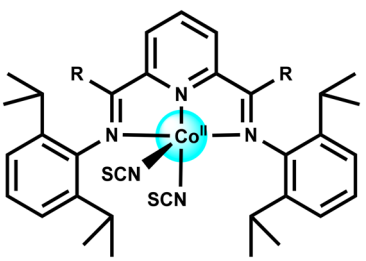

R = Me; Sq. Pyramidal, d = 0.39 Å, D = -28.15 cm^{-1}.
R = Ph; Sq. Pyramidal, d = 0.52 Å, D = -28.22 cm^{-1}.

Fig. 4 Schematic representation of complexes **1a** and **1b**.[67]

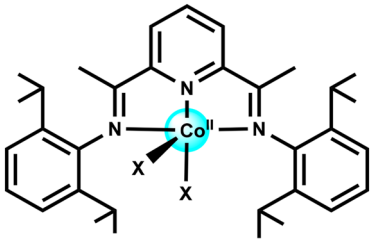

X = SeCN; Sq. Pyramidal, d = 0.39 Å, D = −53.4 cm^{-1}.
X = Cl; Sq. Pyramidal, d = 0.55 Å, D = −55.4 cm^{-1}.
X = Br; Sq. Pyramidal, d = 0.54 Å, D = −32.1 cm^{-1}.

Fig. 5 Schematic representation of complexes **2a–2c**.[68]

U_{eff} = 16 K and $\tau_0 = 3.6 \times 10^{-6}$ s (complex **1a**); U_{eff} = 24 K and $\tau_0 = 5.1 \times 10^{-7}$ s (complex **1b**).[67]

Chandrasekhar and coworkers extended the work for other halides/pseudo-halide ligands with the general formula of $[Co^{II}(L^{1a})(X)_2]$, X = NCSe (**2a**), Cl (**2b**), and Br (**2c**) in a distorted square pyramidal geometry. The degree of distortion varies with the coordinating halide/pseudo-halide ion, influencing the anisotropic parameter D and, consequently, the magnetic properties of the complexes. All three complexes exhibit easy-axis type magnetic anisotropy, with D values of −53.4 cm^{-1} for **2a**, −55.4 cm^{-1} for **2b**, and −32.1 cm^{-1} for **2c** analogues (Fig. 5). Theoretical studies corroborate these findings by explaining the structural distortions in the complexes, wherein the Co(II) center is displaced from the basal plane of the square pyramidal (SPY-5) geometry. This displacement stabilizes the d_{xy} orbital and causes an unsymmetrical occupancy of the nearly degenerate d_{xz} and d_{yz} orbitals, ultimately leading to significant negative magnetic anisotropy. Complexes **2a–2c** experienced field-induced single-ion magnet (SIM) behavior, with magnetic relaxation processes predominantly governed by Raman and direct relaxation pathways.[68] Complexes **2a–2c** exhibited SIM properties with the following signatures: for complex **2a**, magnetization relaxation occurs through both Orbach (U_{eff} = 30.4 K and $\tau_0 = 1.45 \times 10^{-7}$ s) and Raman pathways, 124.7 s^{-1} K^{-n} with n = 2.44 at H_{DC} = 1000 Oe; relaxation for complexes **2b** and **2c** take place through both direct and Raman pathways ($A = 6.05 \times 10^{-13}$ s^{-1} K^{-1} Oe^{-4} and $C = 5.13 \times 10^{-2}$ s^{-1}

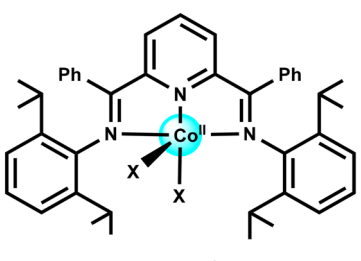

X = Cl; Sq. Pyramidal, d = 0.57 Å, D = −72 cm^{-1}.
X = Br; Sq. Pyramidal, d = 0.54 Å, D = −67 cm^{-1}.
X = I; Sq. Pyramidal, d = 0.46 Å, D = −25 cm^{-1}.

Fig. 6 Schematic representation of complexes **3a–3c**.[69]

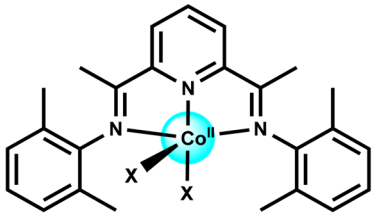

X = **Cl**,TBP ^{d} = 0.01 Å, D = 50 cm^{-1}.
= **Br**, TBP ^{d} = 0.01 Å, D = 40 cm^{-1}.
= **I**, Sq. Pyramidal, ^{d} = 0.43 Å, D = -26 cm^{-1}.

Fig. 7 Schematic representation of complexes **4a**–**4c**.[70]

K^{-n} with n = 6.92 for **2b** and $A = 1.30 \times 10^{-12}$ s^{-1} K^{-1} Oe^{-4} and $C = 4.87 \times 10^{-3}$ s^{-1} K^{-n} with n = 9.15 for **2c**) at H_{DC} = 3000 Oe.

Very recently, Shanmugam and coworkers have further extended the strategy using the phenyl analogue of bis(imino)pyridine NNN-pincer ligand (L^{1b}). They have reported three Co(II) complexes of the general formula of $[Co^{II}(L^{1b})(X)_2]$ [X = Cl (**3a**), Br (**3b**) and I (**3c**)] (Fig. 6). In all these complexes, Co(II) is in a distorted square pyramidal geometry and lies above the basal plane of the square pyramid. All three complexes display easy-axis magnetic anisotropy. The magnitude of the axial zero-field splitting parameter (D) was quantitatively determined using cantilever torque magnetometry, yielding values of −72 cm^{-1} for complex **3a**, −67 cm^{-1} for complex **3b**, and −25 cm^{-1} for complex **3c**. These findings are further corroborated by magnetic susceptibility and EPR measurements. Magnetization relaxation dynamics for these complexes indicate field-induced slow relaxation behavior, predominantly governed by the Raman and direct processes (details are included in the table). The presence of easy axis magnetic anisotropy and the mechanistic insights into the relaxation processes were rationalized through theoretical calculations.[69]

Song Gao and coworkers reported an analogous series of penta-coordinated complexes using a similar bis(imino) pyridine NNN-pincer ligand (L^{1c}) $[Co(L^{1c})X_2]$ [X = Cl (**4a**), Br (**4b**) and I (**4c**)] by changing the halide ligands (Fig. 7).

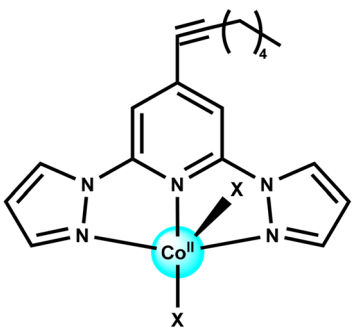

X = Cl, Sq. Pyramidal, ^{d} = 0.56 Å, D = 151 cm^{-1}.

Fig. 8 Schematic representation of complex **5a**.[71]

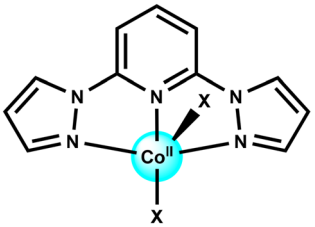

X = Cl, Square Pyramidal, ^{d} = 0.62 Å.
= **NCO, TBP,** ^{d} = 0.66 Å, D = 40.92 cm^{-1}.
= **NCS, TBP**, ^{d} = 0.62 Å, D = 38.4 cm^{-1}.

Fig. 9 Schematic representation of complexes **5b**–**5d**.[73]

Magnetic and spectroscopic measurements led to zero-field splitting (ZFS) parameters: D = 50 cm^{-1} and E = 10 cm^{-1} for complex **4a**, D = 40 cm^{-1} and E = 6 cm^{-1} for complex **4b**, and D = −26 cm^{-1} and E = 7 cm^{-1} for complex **4c**. Nevertheless, all these complexes exhibit field induced SIM behavior with the following parameters: U_{eff} = 29 K and $\tau_0 = 8.3 \times 10^{-7}$ s at H_{DC} = 1000 Oe for **4a**, U_{eff} = 22 K and $\tau_0 = 9.2 \times 10^{-7}$ s at H_{DC} = 2000 Oe for **4b** and U_{eff} = 12 K and $\tau_0 = 7.5 \times 10^{-6}$ s at H_{DC} = 2000 Oe for **4c**.[70]

Boča and coworkers reported square pyramidal based $[CoL^{2a}Cl_2]$ (**5a**) with a tridentate pyridine-based 2,6-bis(pyrazol-1-yl)pyridine ligand (Fig. 8). Complex **5a** exhibited multiple relaxation of magnetization with

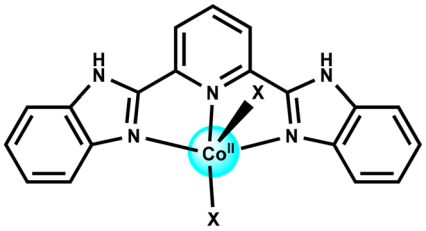

X = **Cl, Square Pyramid**, ^{d} = 0.40 Å, D = 14.5 cm^{-1}.
= **Br, Square Pyramid**, ^{d} = 0.40 Å, D = 8.4 cm^{-1}.
= **NCS, Square Pyramid**, ^{d} = 0.54 Å, D = 10.7 cm^{-1}.

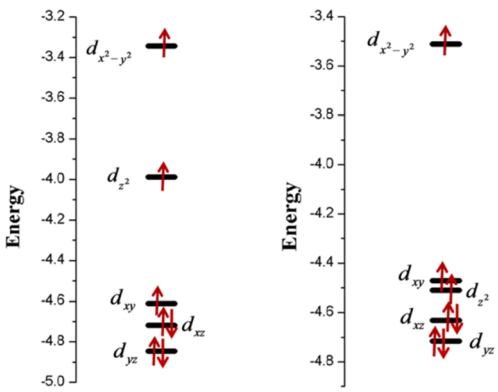

Fig. 10 Schematic representation of complexes **6a**–**6c** (top)[74] and DFT-calculated electronic configurations and d-orbital energy level diagrams for complexes **6a** (bottom left) and **6b** (bottom right), adapted/reproduced from ref. 74 with permission from American Chemical Society,[74] copyright 2017.

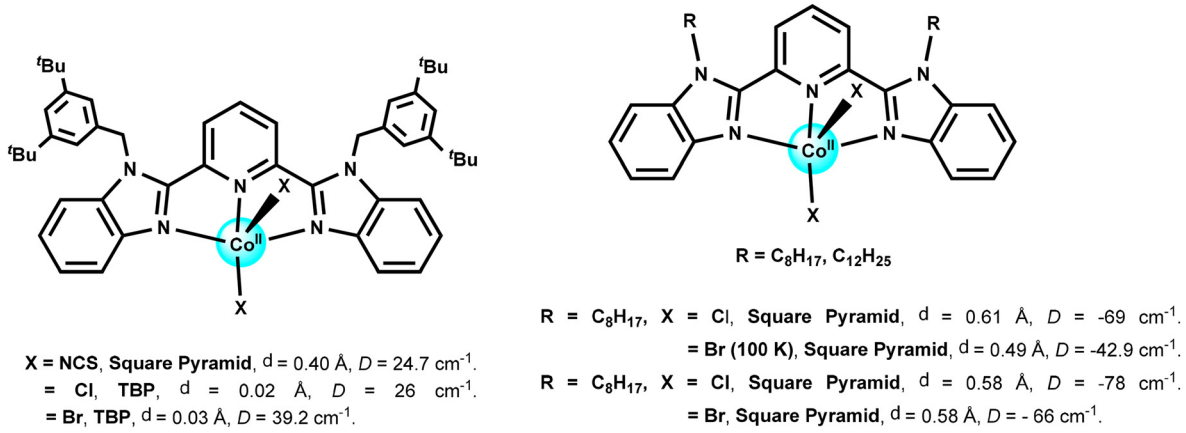

Fig. 11 Schematic representation of complexes **7a**–**7c** (left) and **7d**–**7g** (right).[75,76]

remarkably high single-ion magnetic anisotropy, characterized by an axial zero-field splitting (D) of 151 cm^{-1} and a rhombic component (E) of 11.6 cm^{-1}.[71] The magnetization relaxation details at H_{DC} = 2000 Oe through multiple pathways for **5a** are as follows: Orbach with U_{eff} = 13.5 K and $\tau_0 = 1.35 \times 10^{-7}$ s, direct with $A = 5.2 \times 10^6$ T^{-2} K^{-1} s^{-1}, and Raman with $C = 1.0 \times 10^{-3}$ K^{-4} s^{-1} for n = 4. Theoretical calculations confirm large magnetic anisotropy in complex **5a**. The possible reason could be the involvement of four Kramers doublets (KDs) rather than just two due to the comparable energy gaps among those states as predicted by the calculations.[72] Subsequent studies by the group demonstrated that altering the carbon chain length at the *para* position of the pyridine ring has a minimal impact on magnetic relaxation behavior.[72]

Świtlicka and coworkers extended the work by a small modification in the ligand to report three pentacoordinate cobalt(II) complexes of the type $[Co(L^{2b})X_2]$, where L^{2b} = 2,6-bis(pyrazol-1-yl)pyridine and X = Cl^- (**5b**), NCS^- (**5c**), and NCO^- (**5d**) (Fig. 9). Notably, changing the anions led to the change in the geometry from square pyramidal to intermediate between square pyramidal and trigonal bipyramidal, with τ values of 0.10, 0.36, and 0.46, respectively. These complexes possess large easy plane magnetic anisotropy (D) values of 38.4 cm^{-1} and 40.92 cm^{-1} for complexes **5c** and **5d**. These complexes display slow magnetic relaxation under an applied field, showing multiple relaxation modes.[73] Relaxation parameters for complexes **5b** and **5d** were extracted as follows: Orbach with U_{eff} = 49 K and $\tau_0 = 1.4 \times 10^{-8}$ s, and Raman with C = 2618 K^{-4} s^{-1} for n = 0.8 at H_{DC} = 3500 Oe for complex **5b** and Orbach with U_{eff} = 25.3 K and $\tau_0 = 4.5 \times 10^{-7}$ s, and Raman with C = 128 K^{-4} s^{-1} for n = 2.4 at H_{DC} = 2000 Oe for complex **5d**.

Konar and coworkers reported three pentacoordinate Co^{II} complexes $[Co(L^3)Cl_2]$ (**6a**), $[Co(L^3)Br_2]$ (**6b**), and $[Co(L^3)(NCS)_2]$ (**6c**) using the L^3 = 2,6-bis(2-benzimidazolyl)pyridine ligand. Complexes **6a** and **6b** possess a distorted square pyramidal geometry whereas complex **6c** is in a trigonal

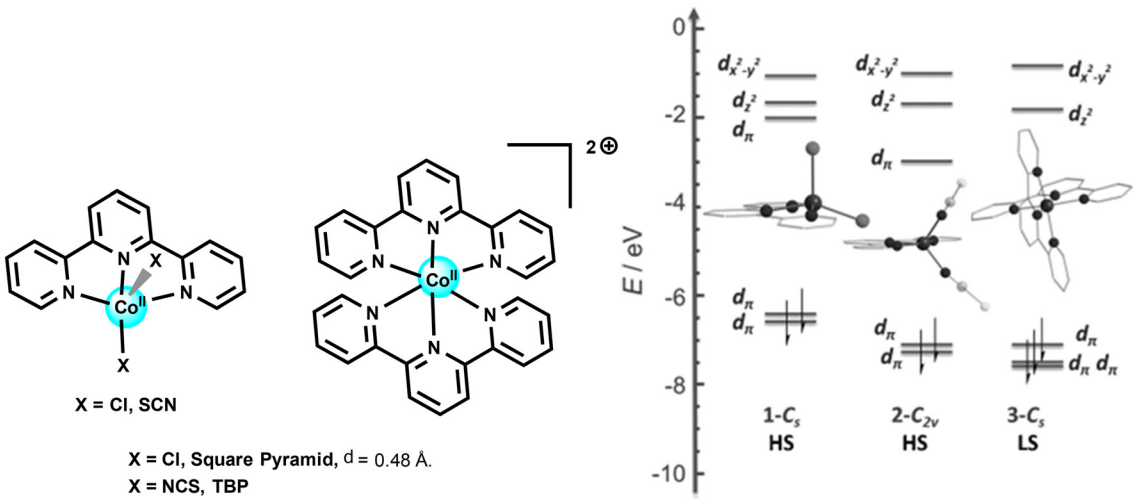

Fig. 12 Schematic representation of complexes **8a**–**8c** (left)[77] and energy-level diagram depicting selected β-spin frontier molecular orbitals of **8a**, **8b**, and **8c** (right), adapted/reproduced from ref. 77 with permission from Wiley,[77] copyright 2013.

Table 1 Summary of the reported five-coordinate Co(II)-SIMs with the molecular formula of $(NNN)CoX_2$

Complex	CShM (4py)	CShM (3bpy)	τ^5	D (cm^{-1})	E (cm^{-1})	H_{dc} (T)	U_{eff} (K)	τ_0 (s)	C (K^{-n} s^{-1})	n	A (Hz K^{-1} Oe^{-4})	Ref.
$[Co(L^{1a})(NCS)_2]$ (**1a**)	1.62	6.40	0.27	−28.15	—	0.2	16	3.6×10^{-6}	—	—	—	67
$[Co(L^{1b})(NCS)_2]$ (**1b**)	1.67	4.65	0.034	−28.22	—	0.2	24	5.1×10^{-7}	—	—	—	67
$[Co^{II}(L^{1a})(NCSe)_2]$ (**2a**)	1.592	6.463	0.25	−53.4	—	0.1	30.4	1.45×10^{-7}	124.7	2.44	—	68
$[Co^{II}(L^{1a})(Cl)_2]$ (**2b**)	1.811	6.847	0.16	−55.4	—	0.3	—	—	5.13×10^{-2}	6.92	6.05×10^{-13}	68
$[Co^{II}(L^{1a})(Br)_2]$ (**2c**)	2.219	7.188	0.18	−32.1	—	0.3	—	—	4.87×10^{-3}	9.15	1.30×10^{-12}	68
$[Co(L^{1b})(Cl)_2]$ (**3a**)	2.225	5.607	0.018	−72	—	—	—	—	3.46×10^5 (Hz)	—	$1.\ 6 \times 10^{-5}$ Hz Oe^{-2} K^{-1}	69
$[Co(L^{1b})(Br)_2]$ (**3b**)	2.611	5.988	0.04	−67	—	—	—	—	4.1×10^5 (Hz)	—	2.02×10^{-4} Hz Oe^{-2} K^{-1}	69
$[Co(L^{1b})(I)_2]$ (**3c**)	3.329	6.360	0.39	−25	—	—	—	—	1.7×10^6 (Hz)	—	$1.\ 2 \times 10^{-4}$ Hz Oe^{-2} K^{-1}	69
$[Co(L^{1c})Cl_2]$ DCE (**4a**)	4.02	2.55	0.39	50.0	10	0.1	29	8.3×10^{-7}	—	—	—	70
$[Co(L^{1c})Br_2]$ MeCN (**4b**)	3.88	2.90	0.38	40.0	6	0.2	22	9.2×10^{-7}	—	—	—	70
$[Co(L^{1c})I_2]$ DCE (**4c**)	3.25	6.33	0.37	−26.0	7	0.2	12	7.5×10^{-6}	—	—	—	70
$[Co(L^{2a})Cl_2]$ (**5a**)	1.90	5.17	0.010	151	—	0.2	13.5	1.35×10^{-7}	1.0×10^{-3}	4	5.2×10^6 T^{-2} K^{-1} s^{-1}	71
$[Co(L^{2b})Cl_2]$ (**5b**)	2.08	4.14	0.10	—	—	0.35	49	1.4×10^{-8}	2618	0.8	—	73
$[Co(L^{2b})(NCS)_2]$ (**5c**)	4.06	3.07	0.36	48.0	—	0.4	—	—	—	—	—	73
$[Co(L^{2b})(NCO)_2]$ (**5d**)	5.97	4.00	0.46	30.0	—	0.2	25.3	4.5×10^{-7}	128	2.4	—	73
$[Co(L^{2a'})Cl_2]$ (**5e**)	2.26	3.81	0.15	61.9	—	0.2	31.3	0.50×10^{-3}	—	—	2.53×10^4	72
$[Co(L^{2a'})Cl_2]$ (**5f**)	3.46	2.83	0.35	70.1	—	0.2	14.6	1.07×10^{-7}	—	—	56.1×10^4	72
$[Co(L^{2a'})Cl_2]$ (**5g**)	4.10	2.67	0.41	46.8	—	0.2	40.5	2.12×10^{-3}	1.8	5	0.59×10^4	72
$[CoL(L^{2a'})Cl_2]$ (**5h**)	1.88	6.95	0.19	87.5	—	0.2	—	4.67×10^{-6}	—	—	—	72
$[Co(L^3)Cl_2]\cdot(MeOH)$ (**6a**)	1.74	6.08	0.27	14.5	0	0.1	19.6	5.8×10^{-5}	—	5.5	—	74
$[Co(L^3)Br_2]\cdot(MeOH)$ (**6b**)	2.16	6.93	0.23	8.4	0	0.1	8.2	3.1×10^{-5}	—	4.6	—	74
$[Co(L^3)(NCS)_2]$ (**6c**)	2.15	3.14	0.29	10.7	1.1×10^{-4}	0.1	9.7	4.6×10^{-5}	—	4.2	—	74
$[Co(L^3)Cl_2]\cdot DMF$ (**6d**)	1.70	5.00	0.42	58.4	—	0.2/0.4	33.2/37.3	13.4×10^{-8}/4.7×10^{-8}	4.27/6.10	5	4.52×10^4/1.22×10^4	78
$[Co(L^3)Br_2]\cdot DMF$ (**6e**)	2.10	5.40	0.017	47.0	0	0.2/0.4	21.0/33.1	5.7×10^{-7}/3.3×10^{-8}	9.31/10.3	5	—	78
$[Co(L^4)(NCS)_2]$ (**7a**)	1.37	5.50	0.30	24.7	8.22	0.15	24.61	5.87×10^{-7}	0.79	6.07	—	75
$[Co(L^4)Cl_2]$ (**7b**)	4.87	1.99	0.55	26.0	8.65	0.15	18.92	2.28×10^{-7}	14.93	5.78		75
$[Co(L^4)Br_2]$ (**7c**)	4.87	2.25	0.20	39.2	13.05	0.125	20.06	7.13×10^{-8}	5.37	7.44	—	75
$[Co(L^{5a})Cl_2]$ (**7d**)	2.403	3.457	0.18	−69		0.1	32.7 (LF) 26.3 (HF)	1.8×10^{-7} (LF) 1.0×10^{-7} (HF)	6.8 (LF) 322 (HF)	2.6 (LF) 9 $\times 10^{-13}$ (HF)	14.3	76
$[Co(L^{5a})Br_2]$ (**7e**)	2.122	4.052	0.12	−78	—	0.1	37	1.19×10^{-7}	—	—	282	76
$[Co(L^{5b})Cl_2]$ (**7f**)	2.215	4.052	0.13	−42.9	—	0.1	33.4 (LF) 45 (HF)	6.2×10^{-8} (LF) 1.9×10^{-10} (HF)	122 (LF) 1953 (HF)	2.3 (LF) 1.3 (HF)	5.3	76

Table 1 *(continued)*

Complex	CShM (4py)	CShM (3bpy)	τ^5	D (cm^{-1})	E (cm^{-1})	H_{dc} (T)	U_{eff} (K)	τ_0 (s)	C (K^{-n} s^{-1})	n	A (Hz K^{-1} Oe^{-4})	Ref.
$[Co(L^{5b})Br_2]$ (**7g**)	2.577	4.789	0.08	−66	—	0.1	31.3	1.16×10^{-7}	0.184	7.07	26	76
$[Co(L^{6a})Cl_2]$ (**8a**)	1.68	5.47	0.052	—	—	0.06/0.56	28.0/4.0	1.07×10^{-6}/ 7.44×10^{-2}	—	—	—	77
$[Co(L^{6a})(NCS)_2]$ (**8b**)	4.48	2.97	0.43	—	—	0.06/0.56	17.0/3.0	5.85×10^{-6}/ 0.11	—	—	—	77
$[Co(L^{6b})Cl_2]$ (**8d**)	1.65	6.05	0.23	−22.2	3.53	0.15	—	—	—	—	—	79
$[Co(L^{7})Cl_2]$ (**9**)	4.10	2.11	0.48	+47.6	—	0.3	—	1.16×10^{-6} (HF)	—	2.3	—	80
$[Co(L^{8a})Cl_2]$ (**10a**)	3.66	2.64	0.43	+45.7	0.24	0.6	—	—	—	—	—	81
$[Co(L^{8b})Cl_2]$ (**10b**)	3.27	2.91	0.31	+38.4	0.31	0.6	—	—	—	—	—	81
$[Co(L^{8c})Cl_2]$ (**10c**)	2.56	3.24	0.48	−43.9	0.26	0.6	—	—	—	—	—	81
$[Co(L^{8d})Cl_2]$ (**10d**)	1.83	6.13	0.089	−41.3	0.0	0.6	22.8	5.23×10^{-9}	83.2	3	849×10^3 T^{-2} K^{-1} s^{-1}	81
$[Co(L^{9a})Cl_2]$ (**11a**)	3.42	2.14	0.51	64.7	0.5	0.2	14.6	6.02×10^{-6}	277.71	1.05	—	82
$[Co(L^{9a})Br_2]$ (**11b**)	4.10	2.31	0.48	45	−6.3	0.2	5.59	7.22×10^{-3}	—	—	—	82
$[Co(L^{9b})(NCS)_2]$ (**11c**)	1.13	6.40	0.16	—	—	0.2	14.7	5.79×10^{-6}	650.9	0.32	—	83
$[Co(L^{9b})Br_2]$ (**11d**)	2.62	3.76	0.19	—	—	0.2	—	—	—	—	—	83
$[Co(L^{10})(NCS)_2]$ (**12**)	1.44	1.93	0.46	−36.8	8.09	0.3	—	—	—	—	—	84
$[Co(L^{11})Cl_2]$ (**13a**)	4.99	2.38	0.55	17.6	2.81	—	—	—	—	—	—	85
$[Co(L^{11})Br_2]$ (**13b**)	1.74	6.46	0.20	30.5	4.57	0.14	—	—	0.77	6.35	3.41×10^{-10}	85
$[Co(L^{11})(NCS)_2]$ (**13c**)	4.96	1.24	0.71	±7.98	±2.31	0.16	—	—	—	—	—	85
$[Co(L^{12a})Cl_2]$ (**14a**)	5.19	2.24	0.79	—	—	—	—	—	—	—	—	86
$[Co(L^{12b})Cl_2]$ (**14b**)	4.73/7.27	1.72/3.01	0.52/0.83	—	—	—	—	—	—	—	—	86

Abbreviations: continuous shape measurements (CShM), square pyramidal geometry (4py), trigonal bipyramidal geometry (3bpy), distortion parameter (τ^5); for an ideal square pyramidal geometry ($\tau^5 = 0$) and for a trigonal bipyramidal geometry ($\tau^5 = 1$), the obtained D values are from the DC magnetic measurements (experimentally obtained), U_{eff} is the effective energy barrier for the magnetization reversal, τ_0 is the relaxation time corresponding to the reversal, H_{DC} corresponds to the applied DC magnetic field for the dynamic magnetic measurements, and A and C correspond to the direct and Raman relaxation processes, respectively.

bipyramidal geometry. In complexes **6a** and **6b**, the Co(II) ion lies above the basal plane of the square pyramid by 0.40 Å. In contrast, in complex **6c**, the Co(II) ion fits in the plane of the L^3 ligand, where one pyridyl nitrogen and two thiocyanate ligands form the equatorial plane of the trigonal bipyramid. All these complexes exhibit easy-plane magnetic anisotropy with D values of 14.5, 8.4, and 10.7 cm^{-1} for **6a**, **6b** and **6c**, respectively. The quantification of the zero-field splitting parameter has been corroborated with the aid of theoretical calculations. Theoretical investigations reveal that the positive D value is due to the $d_{xy} \rightarrow d_{x^2-y^2}$ transition for complexes **6a** and **6b**, and $d_{z^2} \rightarrow d_{x^2-y^2}$ excitation for complex **6c**. All these complexes experience a field induced (at H_{DC} = 1000 Oe) single ion magnet behavior with the following characteristics: U_{eff} = 19.6 K and $\tau_0 = 5.8 \times 10^{-5}$ s (**6a**), U_{eff} = 8.2 K and $\tau_0 = 3.1 \times 10^{-5}$ s (**6b**), and U_{eff} = 9.7 K and $\tau_0 = 4.6 \times 10^{-5}$ s (**6c**) (Fig. 10).[74]

Analogous observations were obtained for another series of penta-coordinated complexes $[Co(L^4)X_2]$ (where X = NCS^- for **7a**, X = Cl^- for **7b** and X = Br^- for **7c**) with a slight modification in the ligand L^4 = [2,6-bis(1-(3,5-di-*tert*-butylbenzyl)-1*H*-benzimidazol-2-yl)pyridine] (Fig. 11, left). In complex **7a**, which contains isothiocyanato terminal ligands, a square pyramidal (SPY) geometry was observed with slight deviation toward a vacant octahedral shape. In contrast, the isomorphic and isostructural complexes **7b** and **7c**, featuring chlorido (Cl^-) and bromido (Br^-) ligands respectively, display a distorted trigonal bipyramidal (TBPY) coordination geometry.[75] In contrast, modifying the ligand by introducing a long alkyl

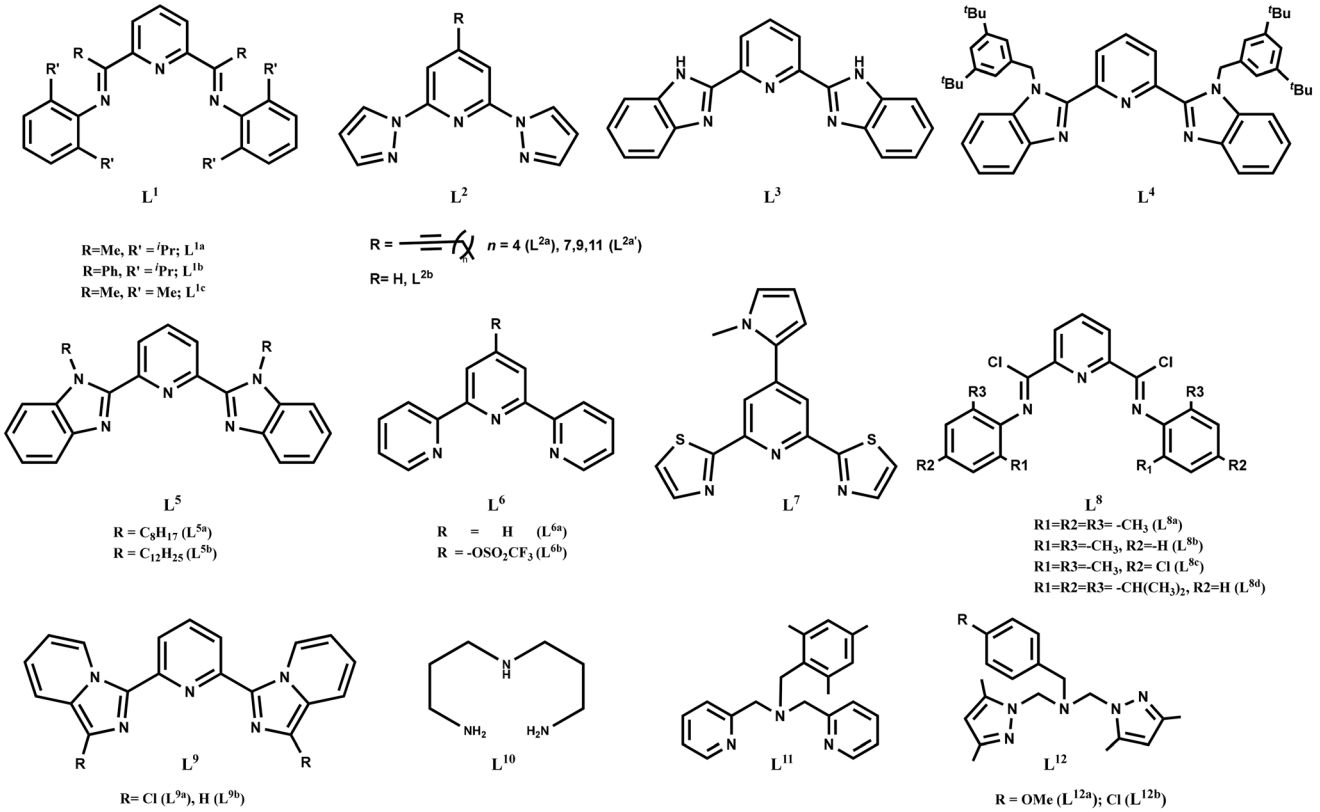

Chart 1 The ligands used to construct the $Co^{II}NNNX_2$-based SIMs mentioned in Table 1.

chain attached to the free N–H group results in the formation of a square pyramidal geometry with reduced distortion toward a trigonal bipyramidal shape (Fig. 11, right).[76] This structural adjustment promotes the development of easy-axis magnetic anisotropy, reflected by a negative D value. Complexes **7a–7c** displayed field induced SIM behavior (at H_{DC} = 1000 Oe) with the following parameters: U_{eff} = 24.61 K and $\tau_0 = 5.87 \times 10^{-7}$ s (**7a**), U_{eff} = 18.92 K and $\tau_0 = 2.28 \times 10^{-7}$ s (**7b**), and U_{eff} = 20.06 K and $\tau_0 = 7.13 \times 10^{-8}$ s (**7c**). Complexes **7d–7g** displayed analogous relaxation characteristics to **7a–7c**; however, a double relaxation process was found to be operative for the Orbach process in two different frequency domains (low frequency and high frequency) as mentioned in the table.

Murugesu and coworkers explored the influence of variations in the ligand field on both slow magnetic relaxation and spin crossover (SCO) behavior in mononuclear Co(II) complexes. They investigated two five-coordinate compounds—$[Co(L^{6a})Cl_2]$ (**8a**) and $[Co(L^{6a})(NCS)_2]$ (**8b**), as well as one six-coordinate complex, $Co(L^{6a})_2$ (**8c**) (Fig. 12). In complex **8a**, the Co(II) ion was displaced by 0.48 Å above the basal plane formed by the three nitrogen atoms of the terpyridine ligand, resulting in a distorted square pyramidal geometry. Conversely, in **8b**, the Co(II) center lies within the terpyridine plane and adopts a trigonal bipyramidal geometry. The hexacoordinate complex **8c** displayed a distorted octahedral geometry (Fig. 12). Complexes **8a** and **8b** exhibit high-spin Co(II) centers at low temperatures and display field-induced (at H_{DC} = 600 Oe) SMM behavior characterized by slow relaxation of magnetization with the following parameters: U_{eff} = 28 K ($\tau_0 = 1.07 \times 10^{-6}$ s) and 4 K ($\tau_0 = 7.44 \times 10^{-2}$ s) for the fast and slow relaxation processes for **8a** and U_{eff} = 17 K ($\tau_0 = 5.85 \times 10^{-6}$ s) and 3 K (τ_0 = 0.11 s) for the fast and slow relaxation processes for **8b**. Notably, multiple relaxation pathways were observed, indicating the complex magnetic dynamics. In contrast, the octahedral geometry of **8c**—achieved by introducing an additional terpyridine ligand—shifts the system toward spin crossover behavior, with a gradual transition from the high-spin to low-spin state. This shift underscores the high sensitivity of the spin states to

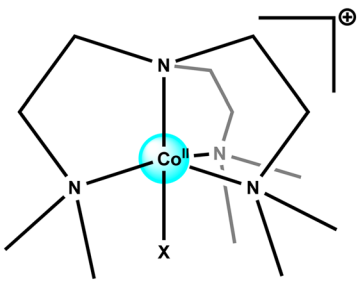

X = Cl, TBP, D = -6.2 cm^{-1}
X = Br, TBP, D = -7.9 cm^{-1}

Fig. 13 Schematic representation of Co^{II} complexes **15a** and **15b**.[87]

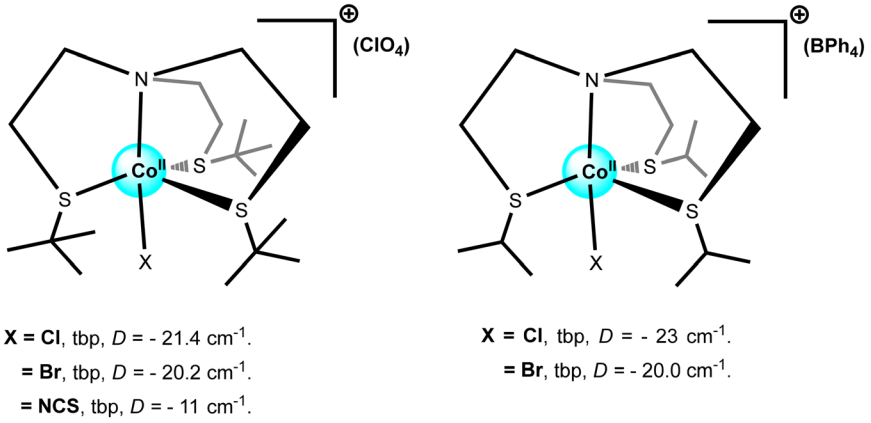

X = Cl, tbp, D = - 21.4 cm^{-1}.
= Br, tbp, D = - 20.2 cm^{-1}.
= NCS, tbp, D = - 11 cm^{-1}.

X = Cl, tbp, D = - 23 cm^{-1}.
= Br, tbp, D = - 20.0 cm^{-1}.

Fig. 14 Schematic representation of Co^{II} complexes **16a–16c** (left) and **16d–16g** (right).[88–90]

changes in the ligand field strength and coordination geometry.[77]

A comprehensive list of all Co(II) complexes featuring $NNNX_2$ coordination environments, along with their detailed magnetic properties, is presented in Table 1, and the corresponding ligand structures are depicted in Chart 1.

Examples of Co(II) SIMs with coordination environments other than $Co(NNN)X_2$

Mallah and co-workers reported complexes $[Co(L^{13})X]^+$ [L^{13} = Me_6tren = hexamethyl tris(aminoethyl)amine; X = Cl (**15a**) and Br (**15b**)] with a trigonal bipyramidal geometry (Fig. 13). Although both complexes possess easy-axis anisotropy, only complex **15a** exhibits hysteresis loops under micro-SQUID measurements performed between 1 K and 30 mK at sweep rates ranging from 0.002 to 0.280 T s^{-1}.[87]

By modifying the ligand framework to elongate the equatorial Co–S bonds, the authors anticipated an enhancement in the magnetic anisotropy. Utilizing this strategy, they synthesized a series of cobalt(II) complexes, $[Co^{II}(NS_3{}^{t}Bu)X]$, L^{14} = $NS_3{}^{t}Bu$ where X = Cl (**16a**), Br (**16b**), or SCN (**16c**), to examine the effect of different axial ligands on magnetic properties (Fig. 14; left). Similar to Me_6tren, the tridentate $NS_3{}^{t}Bu$ ligand enforces a trigonal bipyramidal coordination environment, with the three sulfur atoms occupying the equatorial positions and exhibiting elongated Co–S bond distances. All these complexes exhibited SIM behavior. Notably, complex **16c** displays superior magnetic behavior, primarily due to its C_{3v} symmetry, which eliminates the rhombic zero-field splitting term. This symmetry preserves the purity of the ±3/2 Kramers doublet, thereby suppressing quantum tunneling of magnetization. In contrast, complexes **16a** and **16b** exhibited lower symmetry, leading to the mixing of the ±3/2 and ±1/2 states in the ground doublet, which facilitated faster quantum tunneling pathways.[88] The authors further demonstrated that variations in the aliphatic group attached to the sulfur atoms (ligand L^{15}, complexes **16d–16g**) and changes in the counter anion have only a minimal impact on the magnetic relaxation dynamics in these series of complexes (Fig. 14; right).[89,90]

A tetradentate ligand tris(pyridylmethyl)amine (TPMA; L^{16}) was utilized by Dunbar and co-workers to impose an axial symmetry around the Co(II) centers in the series of complexes $[Co(TPMA)CH_3CN](BF_4)_2$ (**17**); [Co(TPMA)X](X), where X = Cl (**17a**), Br (**17b**), or I (**17c**) (Fig. 15).[91] In all these complexes, the Co(II) center adopts a distorted trigonal bipyramidal geometry. All these complexes (except

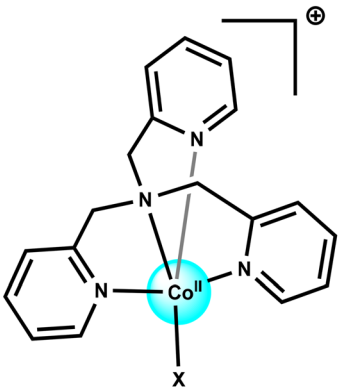

X = BF_4, tbp, D = +9.66 cm^{-1}.
X = Cl, tbp, D = -8.49 cm^{-1}.
X = Br, tbp, D = -7.18 cm^{-1}.
X = I, tbp, D = -7.53 cm^{-1}

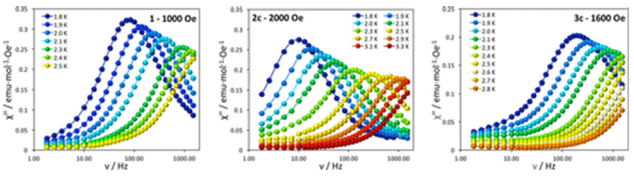

Fig. 15 Schematic representation of Co^{II} complexes **17** and **17a–17c** (top) and field induced AC magnetic data for **17**, **17a** and **17c** at different temperatures (bottom),[91] adapted/reproduced from ref. 91 with permission from American Chemical Society,[91] copyright 2016.

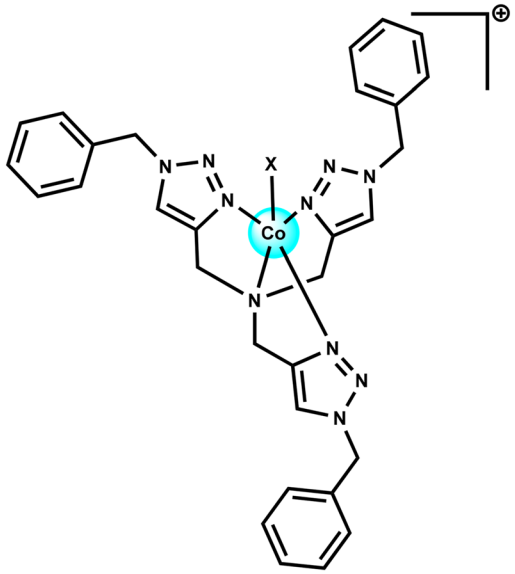

X = Cl; [Co(tbta)Cl](ClO$_4$); tbp, D = - 7.5 cm^{-1}.
X = Br; [Co(tbta)Br](ClO$_4$); tbp, D = - 4.3 cm^{-1}.
X = N$_3$; [Co(tbta)N$_3$]ClO$_4$); tbp, D = - 10.7 cm^{-1}.

Fig. 16 Schematic representation of Co^{II} complexes **18a–18c**.[92,93]

17b) exhibited field-induced single-ion magnet (SIM) behavior. The lack of SIM behavior in **17b** is attributed to the shorter intermolecular Co···Co distances (~6.601 Å), which enhance dipolar interactions and thereby accelerate spin relaxation. Later, Konar and coworkers demonstrated that the counter anion plays a significant role in influencing the magnetic properties of this class of complexes.[92]

Sarkar and coworkers reported a five-coordinate Co(II)–azido complex, [Co(tbta)N$_3$](ClO$_4$) (**18a**) with the Co(II) ion in a TBP geometry (L[17] = tbta = tris[(1-benzyl-1*H*-1,2,3-triazole-4-yl)methyl]amine). The zero-field splitting (ZFS) parameters obtained from the static magnetic data (D = −10.7 cm^{-1}, E/D = 0.22) are in excellent agreement with the D value derived from the Arrhenius analysis of the temperature dependence of the magnetic relaxation. Complex **18a** exhibited field induced slow relaxation of magnetization under an applied external magnetic field of 3000 Oe.[93] Later on, Konar and coworkers extended the work for other halide analogues: [Co(tbta)Cl]·(ClO$_4$)·(MeCN)$_2$·(H$_2$O) (**18b**) and [Co(tbta)Br]·ClO$_4$ (**18c**) (Fig. 16). Both complexes exhibited field-induced SIM behavior under an applied field of 1000 Oe.

Dunbar and coworkers reported six trigonally symmetric divalent Fe, Co, and Ni complexes, stabilized by the rigid, tetradentate, tris-anionic ligand L[18]: (*N*,*N*′,*N*″-[2,2′,2″-nitrilotris(ethane-2,1-diyl)]tris(2,4,6-trimethylbenzenesulfonamide)). A systematic investigation was conducted to compare trigonal mono-pyramidal complexes, (Me$_4$N)[M^{II}(L[18])] (**19**), with their trigonal bipyramidal analogues, (Me$_4$N)[M^{II}(L[18])(OH$_2$)] (**19′**), both experimentally and computationally (Fig. 17). Notably, (Me$_4$N)[Ni(MST)] (**19a**) exhibits an exceptionally large zero-field splitting (D) of −276 cm^{-1}, which is attributed

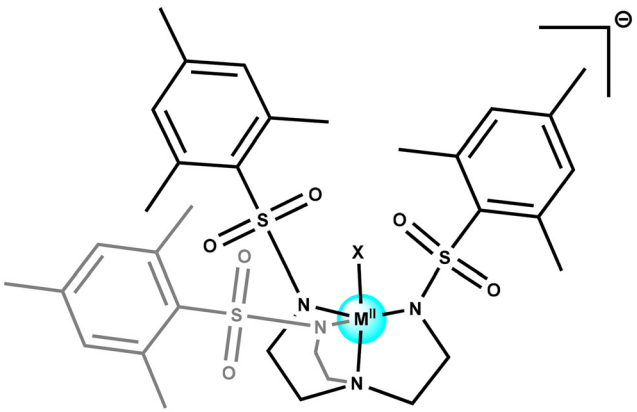

X = None, trigonal monopyramidal, [Co(MST)], D = 33 cm^{-1}.
X = OH$_2$, [Co(MST)(OH$_2$)], TBP, D = 24 cm^{-1}.
X = None, trigonal monopyramidal, [Fe(MST)], D = -31 cm^{-1}.
X = OH$_2$, TBP, [Fe(MST)(OH$_2$)], D = +8.7 cm^{-1}.
X = None, trigonal monopyramidal, [Ni(MST)], D = -276 cm^{-1}.
X = OH$_2$, TBP, [Ni(MST)(OH$_2$)], D = -209 cm^{-1}.

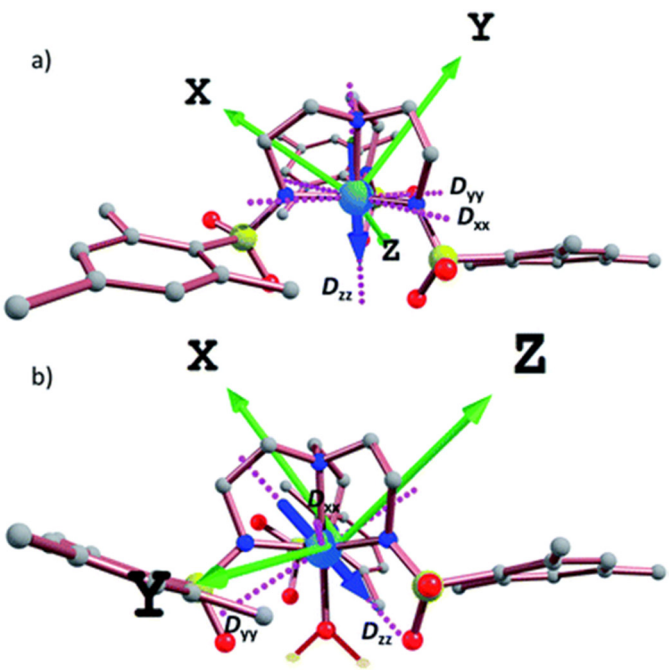

Fig. 17 Schematic representation of complexes **19** and **19′** (left); CASSCF-computed principal magnetic anisotropy axes (D_{xx}, D_{yy}, and D_{zz}) are shown as pink dotted lines for the cobalt complex (a, **19a** and b, **19a′**). The blue arrow highlights the direction and orientation of the D_{zz}, while the green arrows represent the molecular orientation axes (right),[94] adapted/reproduced from ref. 94 with permission from The Royal Society of Chemistry,[94] copyright 2018.

to a very low-lying first excited state. The mono-pyramidal Co and Fe complexes (without OH_2 coordination) showed slow magnetic relaxation under applied dc fields, with U_{eff} values of 45 K (τ_0 = 3.1 × 10^{-9} s) and 63.9 K (τ_0 = 1.98 × 10^{-8} s), respectively. Remarkably, coordination of a single water molecule at the axial site led to a pronounced reduction in D values and suppressed slow relaxation behavior. Computational analysis revealed that water coordination reoriented the D_{zz} axis away from the molecular C_3 axis, diminishing the axial anisotropy. While $(Me_4N)[Co(MST)(OH_2)]$ (**19a′**) retains field-induced relaxation with a reduced U_{eff} of 9.9 K (τ_0 = 1.5 × 10^{-5} s), the aquo–Fe complex loses magnetic relaxation entirely, and the D value in the Ni analog decreases to −209 cm^{-1}. These findings underscore the profound impact of subtle coordination changes on magnetic properties and highlight the potential of trigonal mono-pyramidal geometries for achieving near-record D values in molecular magnets.[94]

Murrie and coworkers demonstrated a strategy to achieve large easy-plane (positive) magnetic anisotropy in a trigonal bipyramidal Co(II) complex, $[Co^{II}Cl_3(L^{19})(HL^{19})]$, 1,4-diazabicyclo[2.2.2]octane (L^{19}, DABCO) (**20**) using a mix of axial and equatorial monodentate ligands (Fig. 18). High-field EPR, frequency-domain magnetic resonance (D = +44.5 cm^{-1}), and *ab initio* methods confirmed the enhanced anisotropy. The complex exhibits zero rhombicity owing to the strict axial symmetry of the C_3-symmetric DABCO ligands and trigonal crystal packing. The complex exhibits slow magnetic relaxation under an applied DC field, which can be explained by Raman, direct, and quantum tunneling processes.[95,96]

Roessler and coworkers demonstrated that interlocked ligands present a strategy for designing metal complexes with predictable and tunable magnetic behavior (Fig. 19). In both the complexes, Co(II) is in a distorted square pyramidal geometry. These rotaxane Co(II) complexes have very large negative D values, D = −78 and −59 cm^{-1} for complexes **21a** and **21b**, respectively. Large negative D values result mainly from strong spin–orbit coupling and small energy gaps between the ground and first excited states, as observed in detailed ligand field and *ab initio* analyses. The study

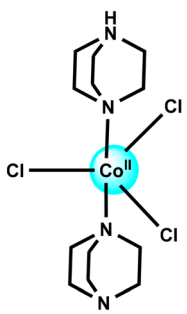

tbp, D = 44.5 cm^{-1}.

Fig. 18 Schematic representation of Co^{II} complexes **20**.[95]

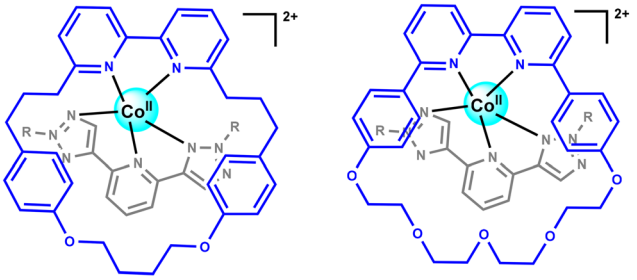

Sq.Pyramidal, D = -78 cm^{-1} Sq.Pyramidal, D = -59 cm^{-1}

Fig. 19 Schematic representation of Co^{II} complexes **21a** and **21b**.[97]

demonstrates that the sign and magnitude of D can be tuned by controlling intramolecular angles and thus the stability of specific d-orbitals, particularly the d_{xy} orbital.[97] Both the complexes exhibit field-induced SIM behavior with the following characteristics: U_{eff} = 156 K and τ_0 = 3.4 × 10^{-5} s (**21a**); U_{eff} = 118 K and τ_0 = 9.8 × 10^{-3} s (**21b**).

Table 2 presents a comprehensive compilation of Co(II) complexes with coordination environments other than $NNNX_2$, along with their detailed magnetic properties, while the corresponding ligand structures are illustrated in Chart 2.

Magneto-structural correlations

Five-coordinate high-spin Co(II) complexes, featuring distorted square pyramidal or trigonal bipyramidal geometries, exhibit notable magnetic anisotropy due to substantial axial zero-field splitting (D) values, reflecting strong spin–orbit coupling and significant interaction between ground and excited states. In these complexes, distorted trigonal bipyramidal geometries generally yield positive D values, while square pyramidal systems can show positive or negative D values depending on how much the Co(II) ion is displaced from the basal plane: a displacement away from the plane produces a negative D value, while co-planarity leads to a positive D value. The degree and nature of this displacement are influenced by factors such as ligand field strength, structural distortions, steric effects from ligand backbones, *etc.*[74,75] Typically, Co(II) SIMs have $|D|$ values between 10 and 120 cm^{-1}. When D is negative (easy-axis anisotropy), it is conducive to slow magnetic relaxation and high blocking temperature, whereas when D is positive (easy-plane anisotropy), it kills SIM behavior by enabling a faster relaxation pathway. Large negative D values (<−40 cm^{-1}) often correspond to axial ligand fields that diminish quantum tunneling and thereby bolster U_{eff} and blocking. Conversely, large positive D values arising from equatorial compression or weak donor fields destabilize the M_s = ±3/2 ground state, lower the barrier height, and are therefore generally correlated to the poor performance of SIMs.

The magneto-structural correlation data for Co(II)-based SIMs reveal that these complexes exhibit moderate to large zero-field splitting (D) values, typically from +151 to −80

Table 2 Summary of five-coordinate Co(II)-SIMs with formulae other than Co(II)(NNN)X_2

Complex	CShM (4py)	CShM (3bpy)	τ^5	D (cm^{-1})	E (cm^{-1})	H_{dc} (T)	U_{eff} (K)	τ_0 (s)	C (K^{-n} s^{-1})	n	A (Hz K^{-1} Oe^{-4})	Ref.
$[Co(L^{13})Cl]ClO_4$ (**15a**)	6.20	0.89	1.03	−6.2	—	0	—	—	—	—	—	87
$[Co(L^{13})Br]Br$ (**15b**)	6.56	1.27	1.03	−7.9	—	—	—	—	—	—	—	87
$[Co(L^{13})(OH_2)](NO_3)_3$ (**15c**)	5.29	0.46	0.96	—	—	0.14	18	9.6×10^{-9}	—	—	—	98
$[Co(L^{14})Cl]ClO_4$ (**16a**)	5.66	0.66	1.00	−21.4	0.24	0.3	—	—	—	—	—	88
$[Co(L^{14})Br]ClO_4$ (**16b**)	4.81/5.18	1.06/0.90	0.87/0.93	−20.2	0.80/2.00	0.3	30.2	4.6×10^{-8}	—	—	—	88
$[Co(L^{14})SCN]ClO_4$ (**16c**)	5.20	0.61	1.04	−11.0	0	0.16	28.7	2.0×10^{-9}	—	—	—	88
$[Co(L^{15})Cl](BPh_4)$ (**16d**)	4.23/4.86	1.06/0.87	0.83/0.91	−19.9	1.5	0.2	46	2.1×10^{-11}	—	—	—	89
$[Co(L^{15})Cl](BPh_4)$ (**16e**)	4.23/4.86	1.06/0.87	0.83/0.91	−19.90	—	0.2	30.6/46.9	1.5×10^{-8}/ 1.6×10^{-11}	0.5/17.0	5	3.01×10^3	89, 90
$[Co(L^{15})Br](BPh_4)$ (**16f**)	5.12/5.65	0.88/0.97	0.88/0.94	−20.0	2.0	0.2	37.8	6.4×10^{-9}	1.12	5	1.20×10^3	90
$[Co(L^{15})Br](ClO_4)$ (**16g**)	4.81/5.18	1.06/0.90	0.87/0.93	−20.20	—	0.3	43.9	2.9×10^{-9}	4.10	5	—	88
$[Co(L^{16})(CH_3CN)](BF_4)_2 \cdot CH_3CN$ (**17**)	5.74	0.98	0.99	9.66	0.26	0.1	21.5	1.7×10^{-8}	0.005	7	—	91
$[Co(L^{16})Cl]Cl$ (**17a**)	6.85	1.81	1.07	−8.49	0	0.04	21.8	2.98×10^{-8}	0.0047	4.4	—	91
$[Co(L^{16})Br]Br$ (**17b**)	7.11	2.28	1.07	−7.18	0	0.16	17.6	8.06×10^{-8}	0.0042	7.4	—	91
$[Co(L^{16})I]I$ (**17c**)	8.18/7.48	3.24/3.09	0.99/1.02	−7.53	1	—	—	—	—	—	—	91
$[Co(L^{16})Cl]Cl \cdot 2.4H_2O$ (**17d**)	7.05/6.80/6.34	1.68/1.70/1.77	1.01/1.04/1.01	−6.95	−1.78	—	—	—	—	—	—	91
$[Co(L^{16})Br]Br \cdot 2.0H_2O$ (**17e**)	7.49/6.80/7.25	2.12/2.15/2.14	1.01/1.02/1.04	−6.30	1.59	—	—	—	—	—	—	91
$[Co(L^{17})N_3]ClO_4 \cdot 3CH_3CN$ (**18a**)	6.20	1.63	1.00	−10.7	−2.35	0.3	28.3	1.6×10^{-8}	—	—	—	93
$[Co(L^{17})Cl] \cdot ClO_4$ (**18b**)	6.10/6.57	1.88/1.84	0.95/1.00	−10.1	1.8	0.1	17.2	7.2×10^{-6}	—	—	—	92
$[Co(L^{17})Br] \cdot ClO_4$ (**18c**)	7.83	2.42	1.10	−4.3	0.03	0.1	7.1	2.1×10^{-6}	—	—	—	92
$(Me_4N)[Co(L^{18})(OH_2)]$ (**19a′**)	5.31	0.69	0.94	24.0	0.001	0.1	9.9	1.5×10^{-5}	0.008	7.2	—	94
$[CoCl_3(L^{19})(HL^{19})]$ (**20**)	5.39	0.02	1.00	44.5	0	0.25	—	—	0.2	5.7	277.9 s^{-1} Oe^{-2} K^{-1}	95
$[Co(L^{20a})](ClO_4)_2$ (**21a**)	0.93	3.32	0.05	−78	—	0	224.5	3.4×10^{-5}	18.415	3.95	113.01	97
$[Co(L^{20b})](ClO_4)_2$ (**21b**)	0.76	4.21	0.07	−59	—	0	169.8	9.8×10^{-3}	6.536	3.82	185.81	97
$[Co(L^{21})(NCS)_2]$ (**22**)	1.906	4.522	0.15	31.8	—	0.2	—	—	—	—	—	99
$[CoL^{22a}](OTf)_2$ (**23a**)	6.146	5.061	0.43	−62.7	9.4	0.1	25	9×10^{-7}	0.6	5.8	13 s^{-1} K^{-1}	100
$[CoL^{22b}](OTf)_2$ (**23b**)	5.659	3.677	0.49	−34.9	10.8	0.12	31	3×10^{-7}	0.3	6.1	70 s^{-1} K^{-1}	100
$[Co^{II}Co^{III}_2(\mu_3\text{-}OH)(\mu\text{-}pz)_4(L^{23})_3]2MeCN$ (**24**)	5.55	0.33	0.89	23.85	4.04	0.1	—	—	2.3	6.6	—	101
$[Co(L^{24})(N_3)]Cl_4$ (**25**)	6.03	0.71	1.05	−7.10	—	0.05	21.5	5×10^{-9}	—	—	—	102
$[(L^{25})_2Co_4Li_8(H_2O)_{12}]$ (**26**)	2.94	0.83	0.69	27.9	−6.3	0.07	21.5	6.2×10^{-8}	—	—	—	103
$[Co(L^{26})(DMSO)Cl_2]$ (**27**)	2.49	2.53	0.54	−17.0	−4.08	0.1	10.4	5.69×10^{-9}	—	—	—	104
$[Co(L^{27})(H_2O)_2]$ (**28**)	5.86	4.79	0.56	16.0	2	0.15	—	—	—	—	—	105
$[Co(L^{27})(L^{28})0.5(H_2O)] \cdot H_2O$ (**29**)	3.62	2.26	0.64	59.0	7	0.3	8.6	1.7×10^{-5}	—	—	—	105
$[Co(L^{29})Cl]ClO_4$ (**30a**)	1.14	3.31	0.33	46.4	10.1	0.1	—	—	—	5.8	—	106

Table 2 *(continued)*

Complex	CShM (4py)	CShM (3bpy)	τ^5	D (cm^{-1})	E (cm^{-1})	H_{dc} (T)	U_{eff} (K)	τ_0 (s)	C (K^{-n} s^{-1})	n	A (Hz K^{-1} Oe^{-4})	Ref.
$[Co(L^{29})Br]ClO_4$ (**30b**)	1.41	3.29	0.35	40.7	9.3	0.1	—	—	—	5.3	—	106
$[Co(L^{30})_2Cl]$·ClO_4 (**31**)	1.37	5.30	0.15	48.5	0.76	0.2	40.3	5.8×10^{-6}	—	4.3	6.9×10^{-16}	107, 108
$[Co^{III}(N_3)_2(L^{31a})(\mu1,1\text{-}N_3)Co^{II}(N_3)]$ (**32a**)	1.91	3.32	0.38	38.7	—	0.4	—	—	—	—	—	109
$[Co^{III}(N_3)_2(L^{31b})(\mu1,1\text{-}N_3)Co^{II}(N_3)]$ (**32b**)	1.87	3.40	0.36	45.7	—	0.4	—	—	—	—	—	109
$[Co(L^{32})Cl](BF_4)$ (**33a**)	0.56	3.04	0.27	45.1	9.9	0.2	7.3	2.7×10^{-6}	—	—	—	110
$[Co(L^{32})Cl](ClO_4)$ (**33b**)	0.85	5.93	0.0062	52.3	10.1	0.2	18.4	3.2×10^{-6}	0.53	4.8	—	110
$[Co(L^{33a})(CH_3CN)](BF_4)_2$ (**34a**)	0.23	5.54	0.00	—	—	0.25	—	—	8.05	4.6	632.53	111
$[Co(L^{33a})(CH_3CN)](PF_6)_2$ (**34b**)	0.04	5.46	0.033	—	—	0.25	—	—	54.33	4	738.02	111
$[Co(L^{33b})(NCO)][B(C_6H_5)_4]$ (**34c**)	0.44	5.66	0.012	—	—	0.1	33.3	1.17×10^{-9}	6.57	5.5	74076.7	112
$[Co(L^{33b})Cl][B(C_6H_5)_4]$ (**34d**)	0.76/0.76	5.62/5.64	0.027/0.023	37.76	0.52	0.08	11.38	4.86×10^{-8}	31.61	7.5	485.4	112
$[Co(L^{33b})Br][B(C_6H_5)_4]$ (**34e**)	1.12/1.08	5.98/5.86	0.019/0.024	37.10	−0.18	0.1	13.52	5.02×10^{-9}	29.83	8.6	42501.6	112
$[Co(L^{34})(MeOH)]$	39.242	33.229	0.63	29.06	—	0.2	—	—	9.50×10^{-3}	8.51	1.86×10^{-12}	113

See Table 1 for the abbreviations.

cm^{-1}, which strongly depend on their coordination geometry and ligand environment (Tables 1 and 2). The magnetic anisotropy of five-coordinate Co(II) SIMs is strongly dependent upon the ligand. The plot of the distortion parameter (τ^5) against the zero-field splitting parameter (D) provides some magneto-structural correlations. This relationship demonstrates how variations in the coordination geometry, ranging from ideal square pyramidal (τ^5 = 0) to trigonal bipyramidal (τ^5 = 1), systematically influence the magnetic anisotropy as reflected in Fig. 20. Complexes with lower τ^5 values (close to 0, ideal square pyramidal coordination) and smaller CShM usually possess negative large values of $|D|$ and easy-axis anisotropy, which predict slow magnetic relaxation. In contrast, higher τ^5 values, corresponding to greater deviations toward trigonal-bipyramidal geometries, favor easy-plane anisotropy or lead to diminished $|D|$ and faster relaxation. Two major horizontal design thresholds are apparent: $\tau^5 \approx 0.22$ (red dashed line) and $|D| \approx 80$ cm^{-1} (blue dashed line). Fig. 20 shows that the complexes with lower τ^5 values (<0.22) and a greater magnitude of $|D|$ value (>80 cm^{-1}) can be called the "optimal" zone, normally easy-axis anisotropy with U_{eff} so large that the magnetization reversal is slow enough without any external field. Complexes with slightly higher τ^5 values ($0.22 < \tau^5 > 0.7$) but still bear large $|D|$ values reside in the "good" zone and represent SIMs with induced fields having moderate blocking behavior. In contrast, the systems exhibiting higher τ^5 values (>0.7) or small $|D|$ (<30 cm^{-1}) show preferential easy-plane anisotropy or relaxation that is fast enough to be dominated by Raman/QTM processes, and thus fail to display robust SIM characteristics. In addition, macrocycles and rigid ligand scaffolds tend to impose axial environments, thereby contributing to a higher U_{eff} with a concomitant reduction in QTM. In contrast, flexible scaffolds lead to distorted geometries and work against the barriers and contribute to a faster relaxation process. Dynamic parameters follow the geometry; the more axial complexes possess greater relaxation times, whereas the distorted structures undergo relaxation *via* shortcut Raman or QTM. Nevertheless, the extent of the zero-field splitting parameter D, and consequently the magnetic relaxation behavior in these complexes, is governed by multiple factors including ligand field strength, coordinating anions, structural distortions around the metal center, and steric effects from organic groups in the secondary coordination sphere. In a nutshell, all of this goes to show that very fine control over the coordination geometry, ligand rigidity, and ligand field strength is essential to the realization of high-performance Co(II)-based SIMs.

It is noteworthy in this context that several complexes listed in Tables 1 and 2, despite possessing $D < 0$, did not exhibit SIM behavior. Complexes with easy-axis ($D < 0$) anisotropy with integer-spin systems and resonant zero-field quantum tunneling relaxation can occur *via* mechanisms such as dipolar interactions, hyperfine interactions, or transverse anisotropy (E). In these scenarios, applying a small static magnetic field may suppress quantum tunneling by eliminating the resonance conditions through the Zeeman

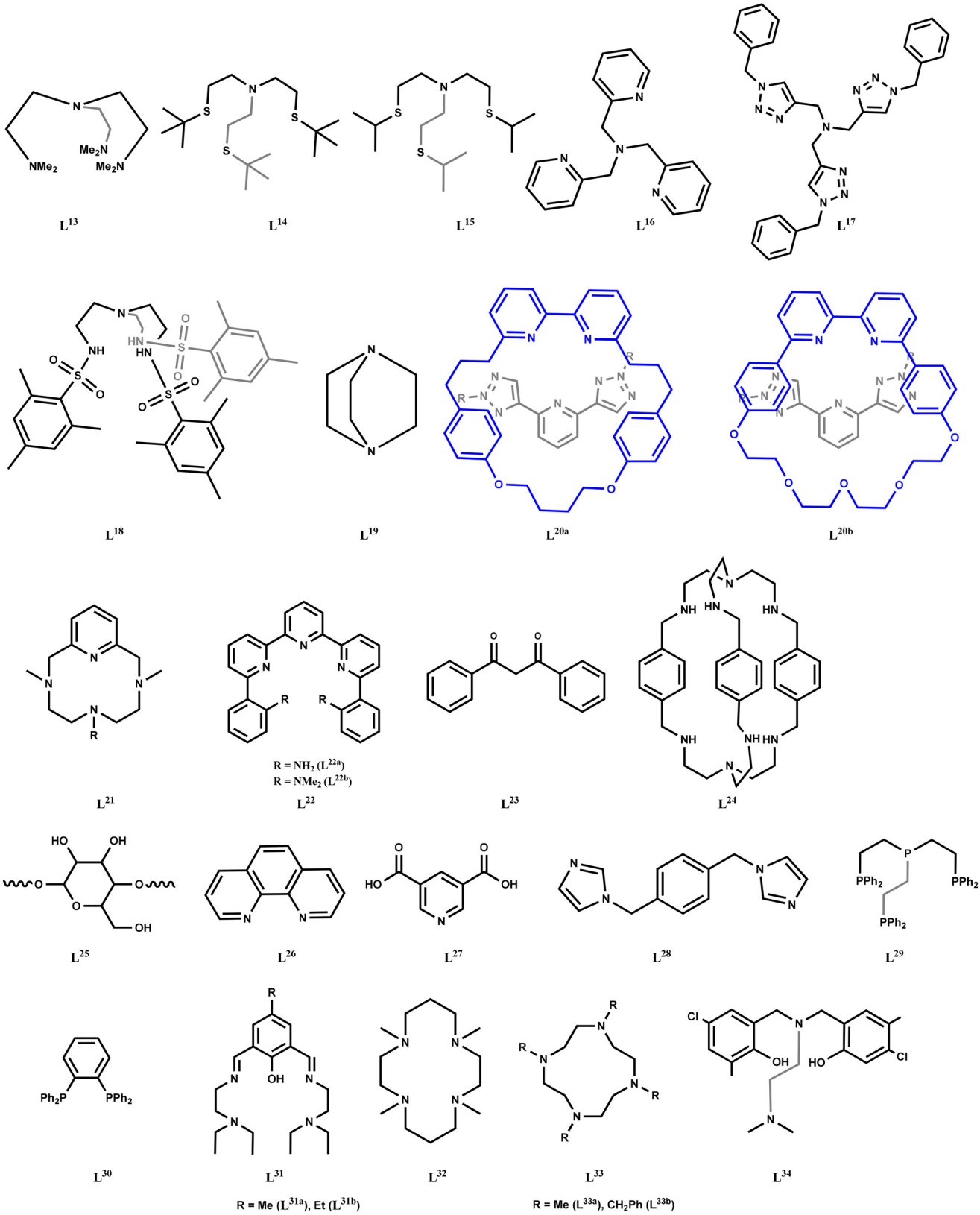

Chart 2 The ligands used to construct Co(II)-based SIMs are listed in Table 2.

effect, thereby permitting the observation of slow, thermally activated magnetic relaxation. Kramers' theorem, however, dictates that for half-integer (non-integer) spin systems with $D < 0$, transverse anisotropy does not lead to level mixing

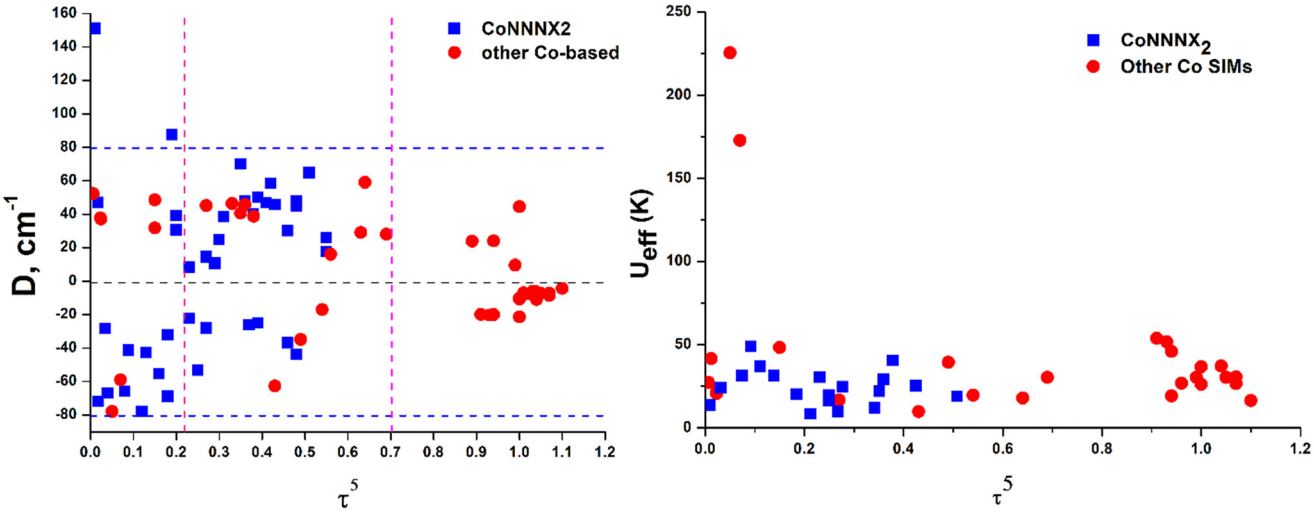

Fig. 20 Correlation between τ^5 and axial zero-field splitting parameter D (left) and plot of U_{eff} against the τ^5 value as obtained from Tables 1 and 2.

that could facilitate tunneling between the ground $\pm M_S$ states. The ground state QTM is therefore restricted. However, structural distortions arising from the ligand field, dipolar interactions, hyperfine interactions, or other perturbations can introduce transverse components that mix the $\pm M_S$ states. This mixing facilitates alternative relaxation pathways by enabling quantum tunneling mechanisms otherwise forbidden in an idealized system.[35,37]

Likewise, several complexes with $D > 0$, as presented in Tables 1 and 2, were found to exhibit SIM behavior. Spin–lattice relaxation in easy-plane with $D > 0$ for half-integer spin systems can happen directly between the ground M_S = ±1/2 states, even without transverse, hyperfine, or dipolar interactions, because the spin–phonon transition is allowed. Thus, fast relaxation would typically be expected in an applied magnetic field. However, if the coupling between the spin and phonons is weak or if there are very few phonons at the right frequencies, the relaxation between M_S = + 1/2 and M_S = −1/2 can be slow to enable the Orbach relaxation process through the higher-energy M_S = ±3/2 levels. This phonon bottleneck effect occurs when phonons available for energy exchange are limited, restricting the spin's ability to relax quickly directly between low-energy levels and allowing alternative relaxation pathways through excited states.[114,115]

Summary and outlook

This review offers an overview of magnetic anisotropy and SIM behavior in five-coordinated cobalt(II) complexes, one of the rapidly expanding classes of 3d-transition metal systems in molecular magnetism. Cobalt(II), with a high-spin d^7 electronic configuration and by virtue of being a Kramers ion, is particularly interesting for SIM design because of its ability to adopt almost any geometry in coordination, strong spin–orbit coupling, and easy tunability on the electronic and geometric fronts. Five-coordinated complexes are uniquely versatile, offering structural fine-tuning that can be harnessed to subtly adjust the Co(II) geometry and ligand field, and thus critically modulate the magnetic relaxation properties.

A central theme of this review is zero-field splitting, which predominantly arises through spin–orbit coupling and controls magnetic anisotropy. The axial ZFS parameter, D, is the principal quantifier of anisotropy; the magnitude and sign of D vary drastically with changes to the coordination environment, modulation of ligand field strength, changes in donor atom identity, distortions in symmetry, or structural perturbations in the geometry around the Co(II) center. Special emphasis was placed on understanding how these factors influence the slow relaxation of magnetization, which is a defining characteristic of SIMs.

The review is organized into two major sections based on the coordination motifs: (i) complexes with an $NNNX_2$-type environment, where N and X represent neutral or anionic donor atoms such as nitrogen, oxygen, sulfur, or halides, and (ii) systems possessing other modes of coordination, which may be trigonal bipyramidal, square pyramidal, or intermediate. Through selected examples, the review illustrates that through rational ligand design *via* rigidification, steric tuning, electronic modification, or symmetry, it is possible to enhance magnetic anisotropy and minimize quantum tunneling of magnetization (QTM).

A series of experimental techniques for determining the magnetic behavior of such systems are discussed, including SQUID magnetometry, AC susceptibility, HF-EPR, *etc.* Furthermore, special emphasis is given to the increasing contributions of theoretical modeling in conjunction with multiconfigurational *ab initio* methods such as CASSCF/NEVPT2 and AILFT. These computational methods are indispensable for the elucidation of electronic structures, interpretation of ZFS parameters, prediction of magnetic behavior, and rational design of new SIM candidates.

Despite the significant progress made in the field, several pathways still exist to develop effective SIMs consisting of 3d transition metals, such as Co(II). The most significant focus over the next few years should be on increasing the blocking temperatures and slowing down rapid relaxation pathways, such as QTM. Five-coordinate Co(II) complexes have suitable geometrical dimensions to address these issues because of their flexible ligand environments and sensitivity to specific geometries. Ongoing and potential research directions include the following:

- Design of higher symmetry ligands that favor uniaxial anisotropy and diminish transverse components that cause QTM.
- Consideration of secondary coordination sphere effects and hydrogen bonding to lock the geometry and modulate the local field.
- Development of rigid and sterically demanding ligands that impose geometries favoring large magnetic anisotropy.
- Utilizing SIMs into solid-state matrices or onto surfaces to fabricate devices for spintronics or quantum computing.
- Responsive SIMs, with magnetic functionalities tunable by external stimuli, like light, redox potential, or pressure.
- Collaborative efforts between theoretical chemists and experimentalists are essential to advance this field by enabling a deeper understanding of structure–property relationships.

The effective exploitation of five-coordinate Co(II)-based single-ion magnets (SIMs) requires seamless integration of synthetic chemistry, advanced characterization techniques, and state-of-the-art theoretical modelling. Ultimately, these systems not only act as model platforms for investigating basic facets of magnetic anisotropy but also stand high on the priority list for future utilization in molecular electronics, high-density data storage, and quantum information science.

Conflicts of interest

There are no conflicts to declare.

Data availability

This article does not present any original experimental data; all data discussed have been adapted from the previously published literature with appropriate copyright permissions.

Acknowledgements

A. D. gratefully acknowledges GITAM University for the MURTI faculty fellowship grant (229MIFF0149). S. D. thanks IITRAM for providing the necessary infrastructure and funding support.

References

1 D. Gatteschi and R. Sessoli, Quantum tunneling of magnetization and related phenomena in molecular materials, *Angew. Chem., Int. Ed.*, 2003, **42**, 268–297.
2 R. Vincent, S. Klyatskaya, M. Ruben, W. Wernsdorfer and F. Balestro, Electronic read-out of a single nuclear spin using a molecular spin transistor, *Nature*, 2012, **488**, 357–360.
3 E. Moreno-Pineda, C. Godfrin, F. Balestro, W. Wernsdorfer and M. Ruben, Molecular spin qudits for quantum algorithms, *Chem. Soc. Rev.*, 2018, **47**, 501–513.
4 E. Moreno-Pineda and W. Wernsdorfer, Measuring molecular magnets for quantum technologies, *Nat. Rev. Phys.*, 2021, **3**, 645–659.
5 E. Coronado, Molecular magnetism: from chemical design to spin control in molecules, materials and devices, *Nat. Rev. Mater.*, 2020, **5**, 87–104.
6 E. Moreno-Pineda and W. Wernsdorfer, Magnetic Molecules as Building Blocks for Quantum Technologies, *Adv. Quantum Technol.*, 2025, **8**, 2300367.
7 D. Gatteschi, R. Sessoli and J. Villain, *Molecular nanomagnets*, Oxford University Press, 2006.
8 R. Boča, Zero-field splitting in metal complexes, *Coord. Chem. Rev.*, 2004, **248**, 757–815.
9 M. Perfetti and J. Bendix, The multiple faces, and phases, of magnetic anisotropy, *Inorg. Chem.*, 2019, **58**, 11875–11882.
10 W. D. W. Horrocks Jr and D. D. W. Hall, Paramagnetic anisotropy, *Coord. Chem. Rev.*, 1971, **6**, 147–186.
11 T. Lis, Preparation, structure, and magnetic properties of a dodecanuclear mixed-valence manganese carboxylate, *Struct. Sci*, 1980, **36**, 2042–2046.
12 R. Sessoli, H. L. Tsai, A. R. Schake, S. Wang, J. B. Vincent, K. Folting, D. Gatteschi, G. Christou and D. N. Hendrickson, High-spin molecules:[Mn12O12 (O2CR) 16 (H2O) 4], *J. Am. Chem. Soc.*, 1993, **115**, 1804–1816.
13 R. Sessoli, D. Gatteschi, A. Caneschi and M. Novak, Magnetic bistability in a metal-ion cluster, *Nature*, 1993, **365**, 141–143.
14 C. J. Milios, A. Vinslava, W. Wernsdorfer, S. Moggach, S. Parsons, S. P. Perlepes, G. Christou and E. K. Brechin, A record anisotropy barrier for a single-molecule magnet, *J. Am. Chem. Soc.*, 2007, **129**, 2754–2755.
15 F. Neese and D. A. Pantazis, What is not required to make a single molecule magnet, *Faraday Discuss.*, 2011, **148**, 229–238.
16 O. Waldmann, A Criterion for the Anisotropy Barrier in Single-Molecule Magnets, *Inorg. Chem.*, 2007, **46**, 10035–10037.
17 N. Ishikawa, M. Sugita, T. Ishikawa, S.-y. Koshihara and Y. Kaizu, Lanthanide Double-Decker Complexes Functioning as Magnets at the Single-Molecular Level, *J. Am. Chem. Soc.*, 2003, **125**, 8694–8695.
18 A. Dey, P. Kalita and V. Chandrasekhar, Lanthanide(III)-Based Single-Ion Magnets, *ACS Omega*, 2018, **3**, 9462–9475.
19 S. G. McAdams, A.-M. Ariciu, A. K. Kostopoulos, J. P. S. Walsh and F. Tuna, Molecular single-ion magnets based on lanthanides and actinides: Design considerations and new advances in the context of quantum technologies, *Coord. Chem. Rev.*, 2017, **346**, 216–239.

20 D. N. Woodruff, R. E. P. Winpenny and R. A. Layfield, Lanthanide Single-Molecule Magnets, *Chem. Rev.*, 2013, **113**, 5110–5148.
21 A. K. Bar, P. Kalita, M. K. Singh, G. Rajaraman and V. Chandrasekhar, Low-coordinate mononuclear lanthanide complexes as molecular nanomagnets, *Coord. Chem. Rev.*, 2018, **367**, 163–216.
22 G. Gabarró-Riera, G. Aromí and E. C. Sañudo, Magnetic molecules on surfaces: SMMs and beyond, *Coord. Chem. Rev.*, 2023, **475**, 214858.
23 G. Gabarró-Riera and E. C. Sañudo, Challenges for exploiting nanomagnet properties on surfaces, *Commun. Chem.*, 2024, **7**, 99.
24 A. K. Bar, C. Pichon and J.-P. Sutter, Magnetic anisotropy in two- to eight-coordinated transition–metal complexes: Recent developments in molecular magnetism, *Coord. Chem. Rev.*, 2016, **308**, 346–380.
25 S. Gómez-Coca, D. Aravena, R. Morales and E. Ruiz, Large magnetic anisotropy in mononuclear metal complexes, *Coord. Chem. Rev.*, 2015, **289–290**, 379–392.
26 J.-P. Sutter, V. Béreau, V. Jubault, K. Bretosh, C. Pichon and C. Duhayon, Magnetic anisotropy of transition metal and lanthanide ions in pentagonal bipyramidal geometry, *Chem. Soc. Rev.*, 2022, **51**, 3280–3313.
27 A. Palii, B. Tsukerblat, S. Klokishner, K. R. Dunbar, J. M. Clemente-Juan and E. Coronado, Beyond the spin model: exchange coupling in molecular magnets with unquenched orbital angular momenta, *Chem. Soc. Rev.*, 2011, **40**, 3130–3156.
28 P. Shukla, S. Das, P. Bag and A. Dey, Magnetic materials based on heterometallic CrII/III–LnIII complexes, *Inorg. Chem. Front.*, 2023, **10**, 4322–4357.
29 S. K. Gupta, S. Dey, T. Rajeshkumar, G. Rajaraman and R. Murugavel, Deciphering the Role of Anions and Secondary Coordination Sphere in Tuning Anisotropy in Dy(III) Air-Stable D5h SIMs, *Chem. – Eur. J.*, 2022, **28**, e202103585.
30 G. A. Craig and M. Murrie, 3d single-ion magnets, *Chem. Soc. Rev.*, 2015, **44**, 2135–2147.
31 D. E. Freedman, W. H. Harman, T. D. Harris, G. J. Long, C. J. Chang and J. R. Long, Slow magnetic relaxation in a high-spin iron (II) complex, *J. Am. Chem. Soc.*, 2010, **132**, 1224–1225.
32 M. Murrie, Cobalt(II) single-molecule magnets, *Chem. Soc. Rev.*, 2010, **39**, 1986–1995.
33 J. M. Frost, K. L. M. Harriman and M. Murugesu, The rise of 3-d single-ion magnets in molecular magnetism: towards materials from molecules?, *Chem. Sci.*, 2016, **7**, 2470–2491.
34 P. Kumar Sahu, R. Kharel, S. Shome, S. Goswami and S. Konar, Understanding the unceasing evolution of Co(II) based single-ion magnets, *Coord. Chem. Rev.*, 2023, **475**, 214871.
35 S. Tripathi, A. Dey, M. Shanmugam, R. S. Narayanan and V. Chandrasekhar, in *Organometallic Magnets*, ed. F. P. V. Chandrasekhar, Springer, Amsterdam, 2018, pp. 35–75.
36 A. G. Blackman, E. B. Schenk, R. E. Jelley, E. H. Krenske and L. R. Gahan, Five-coordinate transition metal complexes and the value of τ5: observations and caveats, *Dalton Trans.*, 2020, **49**, 14798–14806.
37 J. Juráková and I. Šalitroš, Co (II) single-ion magnets: synthesis, structure, and magnetic properties, *Monatsh. Chem.*, 2022, **153**, 1001–1036.
38 J. C. Hempel and M. E. Miller, Ground state properties of trigonal prismatic and trigonal bipyramidal d 1, 9, d 2, 8, d 3, 7, and d 5 systems: Effects of trigonal distortion, *J. Chem. Phys*, 1981, **75**, 2959–2970.
39 F. Lloret, M. Julve, J. Cano, R. Ruiz-García and E. Pardo, Magnetic properties of six-coordinated high-spin cobalt (II) complexes: Theoretical background and its application, *Inorg. Chim. Acta*, 2008, **361**, 3432–3445.
40 L. Lang, M. Atanasov and F. Neese, Improvement of ab initio ligand field theory by means of multistate perturbation theory, *J. Phys. Chem. A*, 2020, **124**, 1025–1037.
41 D. M. Mingos and R. Boča, *Magnetic functions beyond the spin-Hamiltonian*, Springer, 2006.
42 S. Gomez-Coca, E. Cremades, N. Aliaga-Alcalde and E. Ruiz, Mononuclear Single-Molecule Magnets: Tailoring the Magnetic Anisotropy of First-Row Transition-Metal Complexes, *J. Am. Chem. Soc.*, 2013, **135**, 7010–7018.
43 K. Bretosh, V. Béreau, F. Heully-Alary, N. Suaud, C. Duhayon, E. Duverger-Nédellec, N. Guihéry and J.-P. Sutter, Engineering first-order spin–orbit coupling in a pentagonal bipyramidal Fe(ii) complex and subsequent SMM behavior, *Inorg. Chem. Front.*, 2025, **12**, 3456–3468.
44 Y.-S. Meng, S.-D. Jiang, B.-W. Wang and S. Gao, Understanding the Magnetic Anisotropy toward Single-Ion Magnets, *Acc. Chem. Res.*, 2016, **49**, 2381–2389.
45 M. Feng and M.-L. Tong, Single Ion Magnets from 3d to 5f: Developments and Strategies, *Chem. – Eur. J.*, 2018, **24**, 7574–7594.
46 A. Sarkar, S. Dey and G. Rajaraman, Role of Coordination Number and Geometry in Controlling the Magnetic Anisotropy in FeII, CoII, and NiII Single-Ion Magnets, *Chem. – Eur. J.*, 2020, **26**, 14036–14058.
47 F. Neese and E. I. Solomon, *Magnetism: Molecules to Materials IV: Nanosized Magnetic Materials*, Wiley-VCH, Weinheim, 2001.
48 H. C. Silva Jr, H. N. S. Menezes, G. B. Ferreira and G. P. Guedes, Rapid and Accurate Prediction of the Axial Magnetic Anisotropy in Cobalt(II) Complexes Using a Machine-Learning Approach, *Inorg. Chem.*, 2023, **62**, 14838–14842.
49 L. A. Mariano, V. H. A. Nguyen, V. Briganti and A. Lunghi, Charting Regions of Cobalt's Chemical Space with Maximally Large Magnetic Anisotropy: A Computational High-Throughput Study, *J. Am. Chem. Soc.*, 2024, **146**, 34158–34166.
50 A. Sarkar, S. Tewary, S. Sinkar and G. Rajaraman, Magnetic Anisotropy in CoIIX4 (X = O, S, Se) Single-Ion Magnets: Role of Structural Distortions versus Heavy Atom Effect, *Chem. – Asian J.*, 2019, **14**, 4696–4704.
51 M. A. Hay, A. Sarkar, G. A. Craig, L. Bhaskaran, J. Nehrkorn, M. Ozerov, K. E. R. Marriott, C. Wilson, G. Rajaraman, S.

Hill and M. Murrie, In-depth investigation of large axial magnetic anisotropy in monometallic 3d complexes using frequency domain magnetic resonance and ab initio methods: a study of trigonal bipyramidal Co(ii), *Chem. Sci.*, 2019, **10**, 6354–6361.

52 P. Comba, G. Rajaraman, A. Sarkar and G. Velmurugan, What controls the magnetic anisotropy in heptacoordinate high-spin cobalt(ii) complexes? A theoretical perspective, *Dalton Trans.*, 2022, **51**, 5175–5183.

53 A. Swain, T. Sharma and G. Rajaraman, Strategies to quench quantum tunneling of magnetization in lanthanide single molecule magnets, *Chem. Commun.*, 2023, **59**, 3206–3228.

54 T. Sharma, R. Rana, A. Swain and G. Rajaraman, Pushing boundaries in single molecule magnets: an ab initio perspective on harnessing higher oxidation states for unprecedented lanthanide SMM performance, *Inorg. Chem. Front.*, 2025, **12**, 5756–5769.

55 J.-L. Liu, Y.-C. Chen and M.-L. Tong, Symmetry strategies for high performance lanthanide-based single-molecule magnets, *Chem. Soc. Rev.*, 2018, **47**, 2431–2453.

56 A. Chakraborty, J. Goura, P. Kalita, A. Swain, G. Rajaraman and V. Chandrasekhar, Heterometallic 3d–4f single molecule magnets containing diamagnetic metal ions, *Dalton Trans.*, 2018, **47**, 8841–8864.

57 J. Juráková and I. Šalitroš, Co(II) single-ion magnets: synthesis, structure, and magnetic properties, *Monatsh. Chem.*, 2022, **153**, 1001–1036.

58 W. Wernsdorfer, N. E. Chakov and G. Christou, Quantum Phase Interference and Spin-Parity in ${\mathrm{Mn}}_{12}$ Single-Molecule Magnets, *Phys. Rev. Lett.*, 2005, **95**, 037203.

59 W. Wernsdorfer, S. Bhaduri, R. Tiron, D. N. Hendrickson and G. Christou, Spin-Spin Cross Relaxation in Single-Molecule Magnets, *Phys. Rev. Lett.*, 2002, **89**, 197201.

60 A. Zabala-Lekuona, J. M. Seco and E. Colacio, Single-Molecule Magnets: From Mn12-ac to dysprosium metallocenes, a travel in time, *Coord. Chem. Rev.*, 2021, **441**, 213984.

61 C. E. Jackson, I. P. Moseley, R. Martinez, S. Sung and J. M. Zadrozny, A reaction-coordinate perspective of magnetic relaxation, *Chem. Soc. Rev.*, 2021, **50**, 6684–6699.

62 Y.-Q. Zhai and Y.-Z. Zheng, Vibronic barrier effect of magnetic relaxation in single-molecule magnets, *J. Mater. Chem. C*, 2021, **9**, 8096–8098.

63 A. Świtlicka, B. Machura, M. Penkala, A. Bieńko, D. C. Bieńko, J. Titiš, C. Rajnák, R. Boča, A. Ozarowski and M. Ozerov, Slow Magnetic Relaxation in Cobalt(II) Field-Induced Single-Ion Magnets with Positive Large Anisotropy, *Inorg. Chem.*, 2018, **57**, 12740–12755.

64 H.-H. Cui, M.-M. Ding, X.-D. Zhang, W. Lv, Y.-Q. Zhang, X.-T. Chen, Z. Wang, Z.-W. Ouyang and Z.-L. Xue, Magnetic anisotropy in square pyramidal cobalt(ii) complexes supported by a tetraazo macrocyclic ligand, *Dalton Trans.*, 2020, **49**, 14837–14846.

65 J.-Y. Wang, Z. Li, L. Zhang, Y.-C. Chen, Z.-Y. Ruan, S.-N. Du, W. Deng, S.-G. Wu, J.-L. Liu and M.-L. Tong, Temperature-Driven Axial-Equatorial Isomerism and Magnetic Relaxation on Low-Spin Co(II) Borohydride Complexes, *Chin. J. Chem.*, 2025, **43**, 423–430.

66 M. Wang, Z. Han, Y. Garcia and P. Cheng, Six-Coordinated CoII Single-Molecule Magnets: Synthetic Strategy, Structure and Magnetic Properties, *ChemPhysChem*, 2024, **25**, e202400396.

67 T. Jurca, A. Farghal, P.-H. Lin, I. Korobkov, M. Murugesu and D. S. Richeson, Single-molecule magnet behavior with a single metal center enhanced through peripheral ligand modifications, *J. Am. Chem. Soc.*, 2011, **133**, 15814–15817.

68 A. Dey, J. Ali, S. Moorthy, J. F. Gonzalez, F. Pointillart, S. K. Singh and V. Chandrasekhar, Field induced single ion magnet behavior in Co II complexes in a distorted square pyramidal geometry, *Dalton Trans.*, 2023, **52**, 14807–14821.

69 V. Thangaraj, D. Sartini, D. Borah, D. Chauhan, V. Sharma, L. Sorace, G. Rajaraman, M. Perfetti and M. Shanmugam, Quantifying Magnetic Anisotropy of Series of Five-Coordinate CoII Ions: Experimental and Theoretical Insights, *Adv. Sci.*, 2025, **12**, 2415624.

70 J.-J. Liu, Y.-S. Meng, I. Hlavička, M. Orlita, S.-D. Jiang, B.-W. Wang and S. Gao, Determination of zero-field splitting in Co 2+ halide complexes with magnetic and far-IR measurements, *Dalton Trans.*, 2017, **46**, 7408–7411.

71 C. Rajnák, J. N. Titiš, O. Fuhr, M. Ruben and R. Boča, Single-molecule magnetism in a pentacoordinate cobalt (II) complex supported by an antenna ligand, *Inorg. Chem.*, 2014, **53**, 8200–8202.

72 C. Rajnák, J. Titiš, J. Miklovič, G. Kostakis, O. Fuhr, M. Ruben and R. Boča, Five mononuclear pentacoordinate Co (II) complexes as field-induced single molecule magnets, *Polyhedron*, 2017, **126**, 174–183.

73 A. Świtlicka, B. Machura, M. Penkala, A. Bienko, D. C. Bienko, J. Titis, C. Rajnák, R. Boca, A. Ozarowski and M. Ozerov, Slow magnetic relaxation in Cobalt (II) field-induced single-ion magnets with positive large anisotropy, *Inorg. Chem.*, 2018, **57**, 12740–12755.

74 A. K. Mondal, T. Goswami, A. Misra and S. Konar, Probing the effects of ligand field and coordination geometry on magnetic anisotropy of pentacoordinate Cobalt (II) single-ion magnets, *Inorg. Chem.*, 2017, **56**, 6870–6878.

75 B. Brachňaková, S. Matejová, J. Moncol, R. Herchel, J. Pavlik, E. Moreno-Pineda, M. Ruben and I. Šalitroš, Stereochemistry of coordination polyhedra vs. single ion magnetism in penta-and hexacoordinated Co (II) complexes with tridentate rigid ligands, *Dalton Trans.*, 2020, **49**, 1249–1264.

76 J. Juráková, J. Dubnická Midlíková, J. Hrubý, A. Kliuikov, V. T. Santana, J. Pavlik, J. Moncoľ, E. Čižmár, M. Orlita, I. Mohelský, P. Neugebauer, D. Gentili, M. Cavallini and I. Šalitroš, pentacoordinate cobalt(ii) single ion magnets with pendant alkyl chains: shall we go for chloride or bromide?, *Inorg. Chem. Front.*, 2022, **9**, 1179–1194.

77 F. Habib, O. R. Luca, V. Vieru, M. Shiddiq, I. Korobkov, S. I. Gorelsky, M. K. Takase, L. F. Chibotaru, S. Hill, R. H. Crabtree and M. Murugesu, Influence of the ligand field on slow magnetization relaxation versus spin crossover in mononuclear cobalt complexes, *Angew. Chem., Int. Ed.*, 2013, **52**, 11290–11293.

78 C. Rajnák, F. Varga, J. Titiš, J. Moncoľ and R. Boča, Field-Supported Single-Molecule Magnets of Type [Co (bzimpy) X2], *Eur. J. Inorg. Chem.*, 2017, **2017**, 1915–1922.

79 R. F. Higgins, B. N. Livesay, T. J. Ozumerzifon, J. P. Joyce, A. K. Rappé and M. P. Shores, A family of related Co (II) terpyridine compounds exhibiting field induced single-molecule magnet properties, *Polyhedron*, 2018, **143**, 193–200.

80 K. Choroba, J. Palion-Gazda, B. Machura, A. Bieńko, D. Wojtala, D. Bieńko, C. Rajnák, R. Boča, A. Ozarowski and M. Ozerov, Large Magnetic Anisotropy in Mono-and Binuclear cobalt (II) Complexes: The Role of the Distortion of the Coordination Sphere in Validity of the Spin-Hamiltonian Formalism, *Inorg. Chem.*, 2024, **63**, 1068–1082.

81 I. Nemec, H. Liu, R. Herchel, X. Zhang and Z. Trávníček, Magnetic anisotropy in pentacoordinate 2, 6-bis (arylazanylidene-1-chloromethyl) pyridine cobalt (II) complexes with chlorido co-ligands, *Synth. Met.*, 2016, **215**, 158–163.

82 Y. Cui, Y. Xu, X. Liu, Y. Li, B. L. Wang, Y. Dong, W. Li and S. Lei, Field-Induced Single-Ion Magnetic Behavior in Two Mononuclear Cobalt (II) Complexes, *Chem. – Asian J.*, 2019, **14**, 2620–2628.

83 Y. Cui, Y. Ge, Y. Li, J. Tao, J. Yao and Y. Dong, Single-ion magnet behavior of two pentacoordinate Co II complexes with a pincer ligand 2, 6-bis (imidazo [1, 5-a] pyridin-3-yl) pyridine, *Struct. Chem.*, 2020, **31**, 547–555.

84 I. Nemec, R. Herchel and Z. Trávníček, Ferromagnetic coupling mediated by Co⋯ π non-covalent contacts in a pentacoordinate Co (II) compound showing field-induced slow relaxation of magnetization, *Dalton Trans.*, 2016, **45**, 12479–12482.

85 J. Acharya, A. Sarkar, P. Kumar, V. Kumar, J. F. Gonzalez, O. Cador, F. Pointillart, G. Rajaraman and V. Chandrasekhar, Influence of ligand field on magnetic anisotropy in a family of pentacoordinate Co II complexes, *Dalton Trans.*, 2020, **49**, 4785–4796.

86 I. Banerjee, A. Jana, S. Singh, J. Marek, E. Del Barco and M. Ali, Two trigonal–bipyramidal cobalt (II) complexes with small magnetic hysteresis: Synthesis, structure and single crystal magnetic studies, *Polyhedron*, 2013, **66**, 162–166.

87 R. Ruamps, L. J. Batchelor, R. Guillot, G. Zakhia, A.-L. Barra, W. Wernsdorfer, N. Guihéry and T. Mallah, Ising-type magnetic anisotropy and single molecule magnet behaviour in mononuclear trigonal bipyramidal Co (II) complexes, *Chem. Sci.*, 2014, **5**, 3418–3424.

88 F. Shao, B. Cahier, E. Riviere, R. Guillot, N. Guihery, V. E. Campbell and T. Mallah, Structural dependence of the ising-type magnetic anisotropy and of the relaxation time in mononuclear trigonal bipyramidal Co (II) single molecule magnets, *Inorg. Chem.*, 2017, **56**, 1104–1111.

89 F. Shao, B. Cahier, N. Guihéry, E. Riviere, R. Guillot, A.-L. Barra, Y. Lan, W. Wernsdorfer, V. E. Campbell and T. Mallah, Tuning the Ising-type anisotropy in trigonal bipyramidal Co (II) complexes, *Chem. Commun.*, 2015, **51**, 16475–16478.

90 F. Shao, B. Cahier, Y. T. Wang, F. L. Yang, E. Rivière, R. Guillot, N. Guihéry, J. P. Tong and T. Mallah, Magnetic Relaxation Studies on Trigonal Bipyramidal Cobalt (II) Complexes, *Chem. – Asian J.*, 2020, **15**, 391–397.

91 T. J. Woods, M. F. Ballesteros-Rivas, S. Gomez-Coca, E. Ruiz and K. R. Dunbar, Relaxation dynamics of identical trigonal bipyramidal Cobalt molecules with different local symmetries and packing arrangements: Magnetostructural correlations and ab inito calculations, *J. Am. Chem. Soc.*, 2016, **138**, 16407–16416.

92 A. K. Mondal, J. Jover, E. Ruiz and S. Konar, Quantitative Estimation of Ising-Type Magnetic Anisotropy in a Family of C3-Symmetric CoII Complexes, *Chem. – Eur. J.*, 2017, **23**, 12550–12558.

93 D. Schweinfurth, M. G. Sommer, M. Atanasov, S. Demeshko, S. Hohloch, F. Meyer, F. Neese and B. Sarkar, The ligand field of the azido ligand: insights into bonding parameters and magnetic anisotropy in a Co (II)–Azido complex, *J. Am. Chem. Soc.*, 2015, **137**, 1993–2005.

94 K. A. Schulte, K. R. Vignesh and K. R. Dunbar, Effects of coordination sphere on unusually large zero field splitting and slow magnetic relaxation in trigonally symmetric molecules, *Chem. Sci.*, 2018, **9**, 9018–9026.

95 M. A. Hay, A. Sarkar, G. A. Craig, L. Bhaskaran, J. Nehrkorn, M. Ozerov, K. E. Marriott, C. Wilson, G. Rajaraman and S. Hill, In-depth investigation of large axial magnetic anisotropy in monometallic 3d complexes using frequency domain magnetic resonance and ab initio methods: a study of trigonal bipyramidal Co (II), *Chem. Sci.*, 2019, **10**, 6354–6361.

96 M. A. Hay, C. J. McMonagle, C. Wilson, M. R. Probert and M. Murrie, Trigonal to pentagonal bipyramidal coordination switching in a Co (II) single-ion magnet, *Inorg. Chem.*, 2019, **58**, 9691–9697.

97 M. Cirulli, E. Salvadori, Z.-H. Zhang, M. Dommett, F. Tuna, H. Bamberger, J. E. M. Lewis, A. Kaur, G. J. Tizzard, J. van Slageren, R. Crespo-Otero, S. M. Goldup and M. M. Roessler, Rotaxane CoII Complexes as Field-Induced Single-Ion Magnets, *Angew. Chem., Int. Ed.*, 2021, **60**, 16051–16058.

98 D. M. P. Cruz, D. N. Woodruff, I.-R. Jeon, I. Bhowmick, M. Secu, E. A. Hillard, P. Dechambenoit and R. Clérac, Switching off the single-molecule magnet properties of the [Co II (Me 6 tren)(OH 2)] 2+ module by complexation with trans-[Ru III (salen)(CN) 2]−, *New J. Chem.*, 2014, **38**, 3443–3448.

99 S. M. Hossain, S. Kamilya, S. Ghosh, R. Herchel, M. A. Kiskin, S. Mehta and A. Mondal, Tuning of Dimensionality

and Nuclearity as a Function of Ligand Field Modulation Resulting in Field-Induced Cobalt (II) Single-Ion Magnet, *Cryst. Growth Des.*, 2023, **23**, 1656–1667.

100 M. Zeng, Z. Ruan, S. Wu and M. Tong, Field-Induced Slow Magnetic Relaxation in Mononuclear Cobalt (II) Complexes Decorated by Macrocyclic pentaaza Ligands, *Molecules*, 2024, **29**, 2810.

101 A. Collet, G. A. Craig, M. J. H. Ojea, L. Bhaskaran, C. Wilson, S. Hill and M. Murrie, Slow magnetic relaxation in a {Co II Co III2} complex containing a high magnetic anisotropy trigonal bipyramidal Co II centre, *Dalton Trans.*, 2018, **47**, 9237–9240.

102 F. El-Khatib, B. Cahier, F. Shao, M. López-Jordà, R. Guillot, E. Rivière, H. Hafez, Z. Saad, J.-J. Girerd and N. Guihéry, Design and magnetic properties of a mononuclear Co (II) single molecule magnet and its antiferromagnetically coupled binuclear derivative, *Inorg. Chem.*, 2017, **56**, 4601–4608.

103 N. Nedelko, A. Kornowicz, I. Justyniak, P. Aleshkevych, D. Prochowicz, P. Krupiński, O. Dorosh, A. Ślawska-Waniewska and J. Lewiński, Supramolecular control over molecular magnetic materials: γ-cyclodextrin-templated grid of cobalt (II) single-ion magnets, *Inorg. Chem.*, 2014, **53**, 12870–12876.

104 I. Nemec, R. Marx, R. Herchel, P. Neugebauer, J. van Slageren and Z. Trávníček, Field-induced slow relaxation of magnetization in a pentacoordinate Co (ii) compound [Co (phen)(DMSO) Cl 2], *Dalton Trans.*, 2015, **44**, 15014–15021.

105 X. Hou, X. Wang, X. Liu, J. Wang, L. Tang and P. Ju, Fine-tuning the effects of auxiliary ligands on two trigonal-bipyramid cobalt (II) complexes exhibiting field-induced slow magnetic relaxation, *New J. Chem.*, 2018, **42**, 8583–8590.

106 A. K. Mondal, J. Jover, E. Ruiz and S. Konar, Investigation of easy-plane magnetic anisotropy in P-ligand square-pyramidal Co II single ion magnets, *Chem. Commun.*, 2017, **53**, 5338–5341.

107 A. K. Mondal, J. Jover, E. Ruiz and S. Konar, Single-ion magnetic anisotropy in a vacant octahedral Co (II) complex, *Dalton Trans.*, 2019, **48**, 25–29.

108 H.-Y. Guo, W.-Q. Lin and J.-D. Leng, Field-Induced Slow Magnetic Relaxation in pentacoordinate Co(II) Complexes: Tuning Magnetic Anisotropy Through Halide Substitution, *Molecules*, 2025, **30**, 2295.

109 S. Mandal, S. Mondal, C. Rajnák, J. Titiš, R. Boča and S. Mohanta, Syntheses, crystal structures and magnetic properties of two mixed-valence Co (III) Co (II) compounds derived from Schiff base ligands: field-supported single-ion-magnet behavior with easy-plane anisotropy, *Dalton Trans.*, 2017, **46**, 13135–13144.

110 A. K. Mondal, A. Mondal and S. Konar, Field induced single ion magnetic behaviour in square-pyramidal Cobalt (II) complexes with easy-plane magnetic anisotropy, *Magnetochemistry*, 2019, **5**, 12.

111 H.-H. Cui, J. Wang, X.-T. Chen and Z.-L. Xue, Slow magnetic relaxation in five-coordinate spin-crossover cobalt (II) complexes, *Chem. Commun.*, 2017, **53**, 9304–9307.

112 H.-H. Cui, Y.-Q. Zhang, X.-T. Chen, Z. Wang and Z.-L. Xue, Magnetic anisotropy and slow magnetic relaxation processes of cobalt (II)-pseudohalide complexes, *Dalton Trans.*, 2019, **48**, 10743–10752.

113 S. S. Massoud, F. A. Mautner, H. Sakiyama, F. R. Louka, N. H. M. Salem, R. C. Fischer, A. Torvisco, T. Guizouarn, G. Velmurugan, P. Comba and F. Pointillart, SMM Behavior in Distorted Trigonal Bipyramidal and Tetrahedral Cobalt(II) Complexes Based on Tripodal Tetradentate Phenolic Amines, *Eur. J. Inorg. Chem.*, 2025, **28**, e202400777.

114 J. M. Zadrozny, J. Liu, N. A. Piro, C. J. Chang, S. Hill and J. R. Long, Slow magnetic relaxation in a pseudotetrahedral cobalt(ii) complex with easy-plane anisotropy, *Chem. Commun.*, 2012, **48**, 3927–3929.

115 S. Gómez-Coca, A. Urtizberea, E. Cremades, P. J. Alonso, A. Camón, E. Ruiz and F. Luis, Origin of slow magnetic relaxation in Kramers ions with non-uniaxial anisotropy, *Nat. Commun.*, 2014, **5**, 4300.